frontiers in Molecular Neuroscience

ORIGINAL RESEARCH
published: 05 November 2018
doi: 10.3389/fnmol.2018.00406

The Impact of ESCRT on $A\beta_{1-42}$ Induced Membrane Lesions in a Yeast Model for Alzheimer's Disease

Gernot Fruhmann[1†], Christelle Marchal[2†‡], Hélène Vignaud[2], Mathias Verduyckt[1], Nicolas Talarek[3], Claudio De Virgilio[4], Joris Winderickx[1] and Christophe Cullin[2]**

[1] Functional Biology, KU Leuven, Leuven, Belgium, [2] Institut de Chimie et Biologie des Membranes et des Nano-objets, University of Bordeaux, CNRS UMR 5248, Pessac, France, [3] Institut de Génétique Moléculaire de Montpellier, University of Montpellier, CNRS, Montpellier, France, [4] Department of Biology, Université de Fribourg, Fribourg, Switzerland

Aβ metabolism plays a pivotal role in Alzheimer's disease. Here, we used a yeast model to monitor $A\beta_{42}$ toxicity when entering the secretory pathway and demonstrate that processing in, and exit from the endoplasmic reticulum (ER) is required to unleash the full $A\beta_{42}$ toxic potential. Consistent with previously reported data, our data suggests that $A\beta_{42}$ interacts with mitochondria, thereby enhancing formation of reactive oxygen species and eventually leading to cell demise. We used our model to search for genes that modulate this deleterious effect, either by reducing or enhancing $A\beta_{42}$ toxicity, based on screening of the yeast knockout collection. This revealed a reduced $A\beta_{42}$ toxicity not only in strains hampered in ER-Golgi traffic and mitochondrial functioning but also in strains lacking genes connected to the cell cycle and the DNA replication stress response. On the other hand, increased $A\beta_{42}$ toxicity was observed in strains affected in the actin cytoskeleton organization, endocytosis and the formation of multivesicular bodies, including key factors of the ESCRT machinery. Since the latter was shown to be required for the repair of membrane lesions in mammalian systems, we studied this aspect in more detail in our yeast model. Our data demonstrated that $A\beta_{42}$ heavily disturbed the plasma membrane integrity in a strain lacking the ESCRT-III accessory factor Bro1, a phenotype that came along with a severe growth defect and enhanced loading of lipid droplets. Thus, it appears that also in yeast ESCRT is required for membrane repair, thereby counteracting one of the deleterious effects induced by the expression of $A\beta_{42}$. Combined, our studies once more validated the use of yeast as a model to investigate fundamental mechanisms underlying the etiology of neurodegenerative disorders.

Keywords: $A\beta_{42}$, amyloid beta, Alzheimer's disease, ESCRT, membrane repair, *Saccharomyces cerevisiae*, yeast

Edited by:
Ralf J. Braun,
University of Bayreuth, Germany

Reviewed by:
Md. Golam Sharoar,
University of Connecticut Health Center, United States
Markus Babst,
The University of Utah, United States

****Correspondence:***
Joris Winderickx
joris.winderickx@kuleuven.be
Christophe Cullin
christophe.cullin@u-bordeaux.fr

[†]These authors have contributed equally to this work

[‡]Co-first authorship

Received: *13 April 2018*
Accepted: *16 October 2018*
Published: *05 November 2018*

Citation:
Fruhmann G, Marchal C, Vignaud H, Verduyckt M, Talarek N, De Virgilio C, Winderickx J and Cullin C (2018) The Impact of ESCRT on $A\beta_{1-42}$ Induced Membrane Lesions in a Yeast Model for Alzheimer's Disease. Front. Mol. Neurosci. 11:406. doi: 10.3389/fnmol.2018.00406

INTRODUCTION

Amyloid β_{1-42} (referred to as $A\beta_{42}$) is an intensively investigated peptide involved in Alzheimer's disease (AD) but beyond its role as a possibly malignant factor, the physiological functions of $A\beta_{42}$ are still speculative. It has been shown that it has a role in activity dependent synaptic vesicle release and there is evidence that it might act as an antimicrobial agent in the brain, but besides that, not much is known about its physiological function (Pearson and Peers, 2006;

Abramov et al., 2009; Kagan et al., 2012; Kumar et al., 2016). Thus, although several efforts have been put in investigating its role in AD, still most of its functions remain elusive. In humans, the membrane bound amyloid precursor protein, APP, is processed in two possible ways: it can enter the non-amyloidogenic pathway or it might be cleaved by β- and γ-secretases in the amyloidogenic pathway thus producing Aβ peptides of lengths between 37 and 43 amino acids (LaFerla et al., 2007). In AD, these peptides are then secreted and form inert extracellular plaques, but monomers and especially small oligomers are transported to several intracellular organelles where they reveal their toxic potential. For instance, strong evidence was found for that $A\beta_{42}$ perturbs proper function of mitochondria through blocking respiration at complex IV, resulting in cells producing more reactive oxygen species (ROS) and eventually apoptotic cell death (Wang et al., 2010; Ittner and Gotz, 2011; Benilova et al., 2012; Jackrel et al., 2014; Alexandrov et al., 2016; Vicente Miranda et al., 2016).

In the past decade, yeast was established as a model organism for studying fundamental aspects related to neurodegenerative disorders such as Huntington's, Parkinson's, or AD (Winderickx et al., 2008; Franssens et al., 2010; Swinnen et al., 2011; Porzoor and Macreadie, 2013; Jiang et al., 2016; Verduyckt et al., 2016; Fruhmann et al., 2017). Since most of the overall cellular architecture and most basic biochemical processes are conserved between mammalian cells and yeast, and given the fact that about 20–30 per cent of all human genes have orthologs in *Saccharomyces cerevisiae* (Foury, 1997; Hamza et al., 2015; Liu et al., 2017), it is obvious that certain disease mechanisms can be studied in this easy to handle model organism. In connection to AD and $A\beta_{42}$, we and others reported that expression of this peptide triggers toxicity in yeast when targeted to the secretory pathway as to mimic its multi-compartment trafficking observed in mammalian systems. This led to the observation that $A\beta_{42}$ expression in yeast alters endocytosis of plasma membrane resident proteins (Treusch et al., 2011; D'Angelo et al., 2013), induces ER-stress and the unfolded protein response (Chen et al., 2017) and triggers mitochondrial dysfunction (D'Angelo et al., 2013; Chen and Petranovic, 2015; Chen et al., 2017). In the studies presented in this paper, we used previously reported constructs (D'Angelo et al., 2013; Vignaud et al., 2013) where the yeast mating type α-prepro factor directs $A\beta_{42}$ into the Golgi. Here, the α-prepro factor is cleaved off, followed by transport of the peptide to the plasma membrane. In addition, the constructs contain a C-terminal linker-GFP tag in order to ensure stable expression and easy localization of $A\beta_{42}$ in the yeast cells. Besides the wild-type $A\beta_{42}$ and the clinical arctic mutant, we also expressed two synthetic mutants generated by random mutagenesis and previously shown to be either more toxic ($A\beta_{42}$G37C) to, or to be moderately toxic ($A\beta_{42}$L34T) compared to $A\beta_{42}$wt (D'Angelo et al., 2013; Vignaud et al., 2013). Using these constructs, we performed genome-wide screenings as to identify $A\beta_{42}$ toxicity modulators. We confirm the previously reported $A\beta_{42}$ toxicity phenotypes and in addition demonstrate that $A\beta_{42}$ introduces membrane lesions that require the ESCRT system in order to become repaired.

MATERIALS AND METHODS

Yeast Strains, Plasmids, and Media

We used the haploid *Saccharomyces cerevisiae* strain BY4741 MATa *his3Δ1 leu2Δ0 met15Δ0 ura3Δ0* and BY4742 MATα *his3Δ1 leu2Δ0 lys2Δ0 ura3Δ0* for all specified experiments. All deletion strains were obtained from the commercial EUROSCARF knock-out library (Y.K.O. collection). For a full list of strains used in this study see **Table 1**.

The pYe plasmids with the galactose inducible, episomal $\alpha A\beta_{42}$-linker-GFP isoforms, the similar $A\beta_{42}$-GFP construct without the α-prepro sequence and the control constructs for expressing of either GFP (ev-GFP) or a α-prepro-GFP fusion (ev-αGFP) were described previously (Tong et al., 2001). The p426-GAL vector (Addgene) was used as additional empty vector (ev) control. For a full list of plasmids used in this study see **Table 2**.

Standard yeast techniques were applied. We used minimal medium containing Yeast Nitrogen Base (YNB) without ammonium sulfate (FORMEDIUM). Supplements were ammonium sulfate (5 g/L; VWR), histidine (100 mg/L; MP Biomedicals), methionine (20 mg/L; Acros Organics), leucine (30 mg/L; FORMEDIUM) and lysine (30 mg/L; FORMEDIUM). Synthetic Drop-Out (SD) medium was used for microscopy and contained YNB with ammonium sulfate and was depleted for either uracil or uracil and leucine (FORMEDIUM). For solid media, 1.5% Difco-agar (BD) was added. Pre-cultures were grown on medium supplemented with 4% glucose and gene expression was induced by washing the cells with medium without sugar followed by transfer to medium supplemented with 2% galactose.

Synthetic Genetic Array and Suppressor screening

The synthetic genetic array (SGA) screening was essentially performed as previously described in Tong et al. (2001). The query strain (MATα *can1Δ::STE*pr-*HIS5*sp *lyp1Δ his3Δ1 leu2Δ0 met15Δ0 ura3Δ0 LYS2*) expressing $\alpha A\beta_{42}$wt-linker-GFP (further designated as $\alpha A\beta_{42}$wt), the $\alpha A\beta_{42}$G37C-linker-GFP (designated $\alpha A\beta_{42}$G37C) or the ev-αGFP was mated with the non-essential deletion mutant array (MATa *target_gene::kanMX4 his3Δ1 leu2Δ0 met15Δ0 ura3Δ0*) on SD plates lacking uracil. Diploids were selected on SD medium lacking uracil but containing G418 (geneticin). Next, sporulation was induced by plating diploids onto sporulation medium containing G418. Then, haploids were selected in two steps. First, spores were plated onto YNB lacking arginine, lysine, and histidine but containing canavanine and thialysine, which ensures uptake of canavanine. This allowed growth of MATa haploids only. In a second step, the selected haploids were grown on YNB lacking uracil, arginine, lysine, and histidine but containing canavanine, thialysine and G418 to select for haploid knock-out mutants still carrying the $\alpha A\beta_{42}$wt, $\alpha A\beta_{42}$G37C, or ev-αGFP plasmids. Growth analysis was performed with the ScreenMill software (Dittmar et al., 2010).

TABLE 1 | Yeast strains used in this study.

Name	Genotype	Source
Query strain (SGA)	MATα *can1Δ::STEpr-HIS5sp lyp1Δ his3Δ1 leu2Δ0 met15Δ0 ura3Δ0 LYS2*	Tong et al., 2001
Deletion mutant strains (SGA)	MATa *Target_gene::kanMX4 his3Δ1 leu2Δ0 met15Δ0 ura3Δ0*	Tong et al., 2001
BY4741	MATa *his3Δ1 leu2Δ0 met15Δ0 ura3Δ0*	Openbiosystems
BY4742	MATα *his3Δ1 leu2Δ0 lys2Δ0 ura3Δ0*	Openbiosystems
JW 12 918	MATa *his3Δ1 leu2Δ0 met15Δ0 ura3Δ0 erv29::kanMX*	Y.K.O. collection
JW 23 168	MATα *his3Δ1 leu2Δ0 lys2Δ0 ura3Δ0 hse1Δ::kanMX*	Y.K.O. collection
JW 23 771	MATα *his3Δ1 leu2Δ0 lys2Δ0 ura3Δ0 vps27::kanMX*	Y.K.O. collection
JW 20 178	MATα *his3Δ1 leu2Δ0 lys2Δ0 ura3Δ0 srn2::kanMX*	Y.K.O. collection
JW 21 184	MATα *his3Δ1 leu2Δ0 lys2Δ0 ura3Δ0 mvb12::kanMX*	Y.K.O. collection
JW 21 335	MATα *his3Δ1 leu2Δ0 lys2Δ0 ura3Δ0 stp22::kanMX*	Y.K.O. collection
JW 22 115	MATα *his3Δ1 leu2Δ0 lys2Δ0 ura3Δ0 vps28::kanMX*	Y.K.O. collection
JW 23 142	MATα *his3Δ1 leu2Δ0 lys2Δ0 ura3Δ0 vps25::kanMX*	Y.K.O. collection
JW 21 849	MATα *his3Δ1 leu2Δ0 lys2Δ0 ura3Δ0 vps36::kanMX*	Y.K.O. collection
JW 22 164	MATα *his3Δ1 leu2Δ0 lys2Δ0 ura3Δ0 snf8::kanMX*	Y.K.O. collection
JW 20 891	MATα *his3Δ1 leu2Δ0 lys2Δ0 ura3Δ0 doa4::kanMX*	Y.K.O. collection
JW 22 100	MATα *his3Δ1 leu2Δ0 lys2Δ0 ura3Δ0 bro1::kanMX*	Y.K.O. collection
JW 22 220	MATα *his3Δ1 leu2Δ0 lys2Δ0 ura3Δ0 vps4::kanMX*	Y.K.O. collection
JW 22 777	MATα *his3Δ1 leu2Δ0 lys2Δ0 ura3Δ0 did2::kanMX*	Y.K.O. collection
JW 24 370	MATα *his3Δ1 leu2Δ0 lys2Δ0 ura3Δ0 vps60::kanMX*	Y.K.O. collection
JW 21 424	MATα *his3Δ1 leu2Δ0 lys2Δ0 ura3Δ0 vta1::kanMX*	Y.K.O. collection
JW 23 123	MATα *his3Δ1 leu2Δ0 lys2Δ0 ura3Δ0 chm7::kanMX*	Y.K.O. collection
JW 20 444	MATα *his3Δ1 leu2Δ0 lys2Δ0 ura3Δ0 ist1::kanMX*	Y.K.O. collection
JW 20 124	MATα *his3Δ1 leu2Δ0 lys2Δ0 ura3Δ0 snf7::kanMX*	Y.K.O. collection
JW 21 479	MATα *his3Δ1 leu2Δ0 lys2Δ0 ura3Δ0 vps24::kanMX*	Y.K.O. collection
JW 22 806	MATα *his3Δ1 leu2Δ0 lys2Δ0 ura3Δ0 vps20::kanMX*	Y.K.O. collection
JW 11 560	MATα *his3Δ1 leu2Δ0 lys2Δ0 ura3Δ0 did4::kanMX*	Y.K.O. collection

TABLE 2 | Plasmids used in this study.

Name	Backbone	Marker	Insert	Source
$\alpha A\beta_{42}$wt	pYe-GAL10 2U	*URA3*	*α-prepro-*$A\beta_{42}$*wt-linker-GFP*	D'Angelo et al., 2013
$\alpha A\beta_{42}$arc	pYe-GAL10 2U	*URA3*	*α-prepro-*$A\beta_{42}$*arc-linker-GFP*	D'Angelo et al., 2013
$\alpha A\beta_{42}$G37C	pYe-GAL10 2U	*URA3*	*α-prepro-*$A\beta_{42}$*G37C-linker-GFP*	D'Angelo et al., 2013
$\alpha A\beta_{42}$G37C-HDEL	pYe-GAL10 2U	*URA3*	*α-prepro-*$A\beta_{42}$*G37C-linker-GFP-HDEL*	Christophe Cullin
$\alpha A\beta_{42}$L34T	pYe-GAL10 2U	*URA3*	*α prepro-*$A\beta_{42}$*L34T-linker-GFP*	D'Angelo et al., 2013
ev-αGFP	pYe-GAL10 2U	*URA3*	*α-prepro-GFP*	D'Angelo et al., 2013
ev-GFP	pYe-GAL10 2U	*URA3*	*GFP*	D'Angelo et al., 2013
Ev	p426-GAL1	*URA3*		Mumberg et al., 1994
pHS12-mCherry	pHS12-ADH1	*LEU2*	*COX4*	Addgene
pYX242-mCherry	pYX242-TPI	*LEU2*	*Kar2*$_{(1-135)}$*-mCherry-HDEL*	Swinnen et al., 2014

In a second so-called suppressor screening, the Euroscarf collection of deletion strains was pooled transformed with αAβ42G37C. Transformants were plated on minimal medium lacking uracil. After incubation, transformants were selected that grew similar as the isogenic wild-type carrying the empty vector control, also when replica plated on SD medium supplemented with casamino acids. Transformants were then used for bar-code PCR sequencing as to identify their corresponding ORF deletion.

Electron Microscopy

Electron microscopic analysis of yeast cells was done similar as previously described (Lefebvre-Legendre et al., 2005). Briefly, pellets of yeast cells were placed on the surface of a copper

EM grid (400 mesh) coated with formvar. Grids were immersed in liquid propane held at −180°C by liquid nitrogen and then transferred in a 4% osmium tetroxide solution in dry acetone at −82°C for 72 h. They were warmed progressively to RT, and washed three times with dry acetone and stained with 1% uranyl acetate. After washing in dry acetone, the grids were infiltrated with araldite (Fluka). Ultra-thin sections were contrasted with lead citrate and observed in an electron microscope (80 kV; 7650; Hitachi) at the EM facility of the Bordeaux Imaging Center.

Growth Profile Analysis and Spot Assays

Cells were grown under non-inducing conditions in 96-well plates shaking at 30°C in a Multiskan GO or Multiskan FC microplate spectrophotometer (Thermo Scientific) to an $OD_{595\ nm}$ or $OD_{600\ nm}$, respectively, of 0.5 to 0.9. Cells were washed with minimal medium containing galactose and diluted to an $OD_{595\ nm}$ or $OD_{600\ nm}$, respectively, of 0.5 after which growth was monitored every 2 h by OD measurement. Four different transformants were taken per experiment and at least three independent experiments were performed. Growth curves were analyzed with GraphPad Prism v7.03, error bars represent standard deviations.

For spot assays, serial dilutions of precultures were spotted on solid medium containing either glucose or galactose and cells were grown at 30°C. The plates were scanned at days 3 to 6.

Cytometry and Fluorescence Microscopy

To monitor plasma membrane disruption with propidium iodide (PI) staining and the formation of ROS by dihydroethidium (DHE) staining, cells were grown in SD medium lacking uracil and containing 4% glucose. Once in exponential phase, the cells were washed with and re-suspended in SD medium without uracil but containing 2% galactose as to induce expression of $\alpha A\beta_{42}$-linker-GFP and control constructs. Flow cytometric analysis was performed on at least four independent transformants with a Guava easyCyte 8HT benchtop flow cytometer (Millipore) after staining with 5 μM PI for 30 min at 30°C and subsequent washing. Data were analyzed with FlowJo v10 and GraphPad Prism 7.03 software packages. Gates were set in FlowJo v10 with single stained ev-αGFP samples. Further statistical analysis was done in GraphPad Prism v7.03. Error bars represent standard deviations and asterisks the significance calculated with an ordinary Two-way ANOVA.

For the FM4-64/CMAC (Thermo Fisher) and Nile Red (Acros) stainings, the cells were grown as described above. After pre-incubating the cells with CAMAC at 30°C for 30 min, FM4-64 stainings were performed as described before (Zabrocki et al., 2005). For the Nile Red staining, the cells were fixed with formaldehyde (4% final concentration) and stained with 2% Nile Red (60 μg/mL stock) for 30 min with shaking at 30°C. Then, the cells were washed twice with PBS and either stored at 4°C or taken immediately for fluorescence microscopy.

For epifluorescence pictures, cells were pre-grown in selective glucose (4%) containing SD medium to exponential phase. After transfer to SD medium containing 2% galactose to induce expression of $\alpha A\beta_{42}$-linker-GFP, the cells were grown at 30°C and pictures were taken after different time intervals using a Leica DM4000B or a DMi8 microscope. For Hoechst stainings, the cells were incubated with 20 nM Hoechst 33342 (Sigma-Aldrich) for 10 min. Pictures were deconvolved with Huygens Essential software (v18.04.0p4 64, Scientific Volume Imaging B.V.) and further processed with the standard FIJI software package (v1.51n) (Schindelin et al., 2012).

Immunological Techniques

Cultures were grown to exponential phase in 4% glucose containing SD medium, transferred to 2% galactose containing medium and grown overnight. Then, three OD units were harvested by centrifugation and protein extracts were prepared by using an alkaline lysis method. The cells were permeabilized with 0.185 M NaOH plus 2% β-mercaptoethanol. After 10 min incubation on ice, trichloroacetic acid (TCA) was added to a final concentration of 5%, followed by an additional 10 min incubation step on ice. Precipitates were collected by centrifugation for 5 min at 13000 *g* and pellets were resuspended in 50 μL of sample buffer (4% sodium dodecyl sulfate, 0.1 M Tris-HCl pH 6.8, 4 mM EDTA, 20% glycerol, 2% β-mercaptoethanol, and 0.02% bromophenol blue) plus 25 μL of 1 M Tris-Base. Samples were separated by standard SDS-PAGE on 12% polyacrylamide gels and further analyzed using standard Western blotting techniques. An anti-GFP primary antibody (Sigma-Aldrich) and anti-Mouse (GAM)-HRP conjugated secondary antibody (Biorad) were used. The ECL method (SuperSignal West Pico or Femto, Thermo Scientific) was used for detection and visualization of the blots was performed with a UVP Biospectrum® Multispectral Imaging System.

RESULTS

αAβ$_{42}$-Linker-GFP Is Toxic in an AD Yeast Model

To date, the exact molecular basis of how $A\beta_{42}$ impacts cell functions remains largely elusive. To address this question, we used a yeast model transformed with plasmids carrying the galactose-inducible *GAL10* promoter to control expression of wild-type or mutant $A\beta_{42}$ that is N-terminally fused to the α-prepro sequence and C-terminally to a linker and GFP (in this paper referred to as $\alpha A\beta_{42}$; **Figure 1A**) (D'Angelo et al., 2013; Vignaud et al., 2013). Besides the wild-type $\alpha A\beta_{42}$ ($\alpha A\beta_{42}$wt), we additionally expressed the clinical E22G arctic mutant ($\alpha A\beta_{42}$arc) that is associated to a familial form of AD as well as the previously described synthetic mutants $\alpha A\beta_{42}$G37C and $\alpha A\beta_{42}$L34T (**Figure 1A**) (D'Angelo et al., 2013; Vignaud et al., 2013). We used three control vectors, i.e., an empty vector allowing for the expression of an α-prepro fused GFP (ev-αGFP), GFP alone (ev-GFP) or an empty vector just carrying the galactose promotor (ev). To disperse concerns about the processing efficacy of the α-prepro factor in the Golgi system, we tested both the BY4741 MATa and BY4742 MATα strains with all control vectors and the aforementioned wild-type and mutant $\alpha A\beta_{42}$-linker-GFP constructs (**Figures 1B–D** and **Supplementary Figure S1**). Albeit the strains transformed with the ev-αGFP control grew somewhat

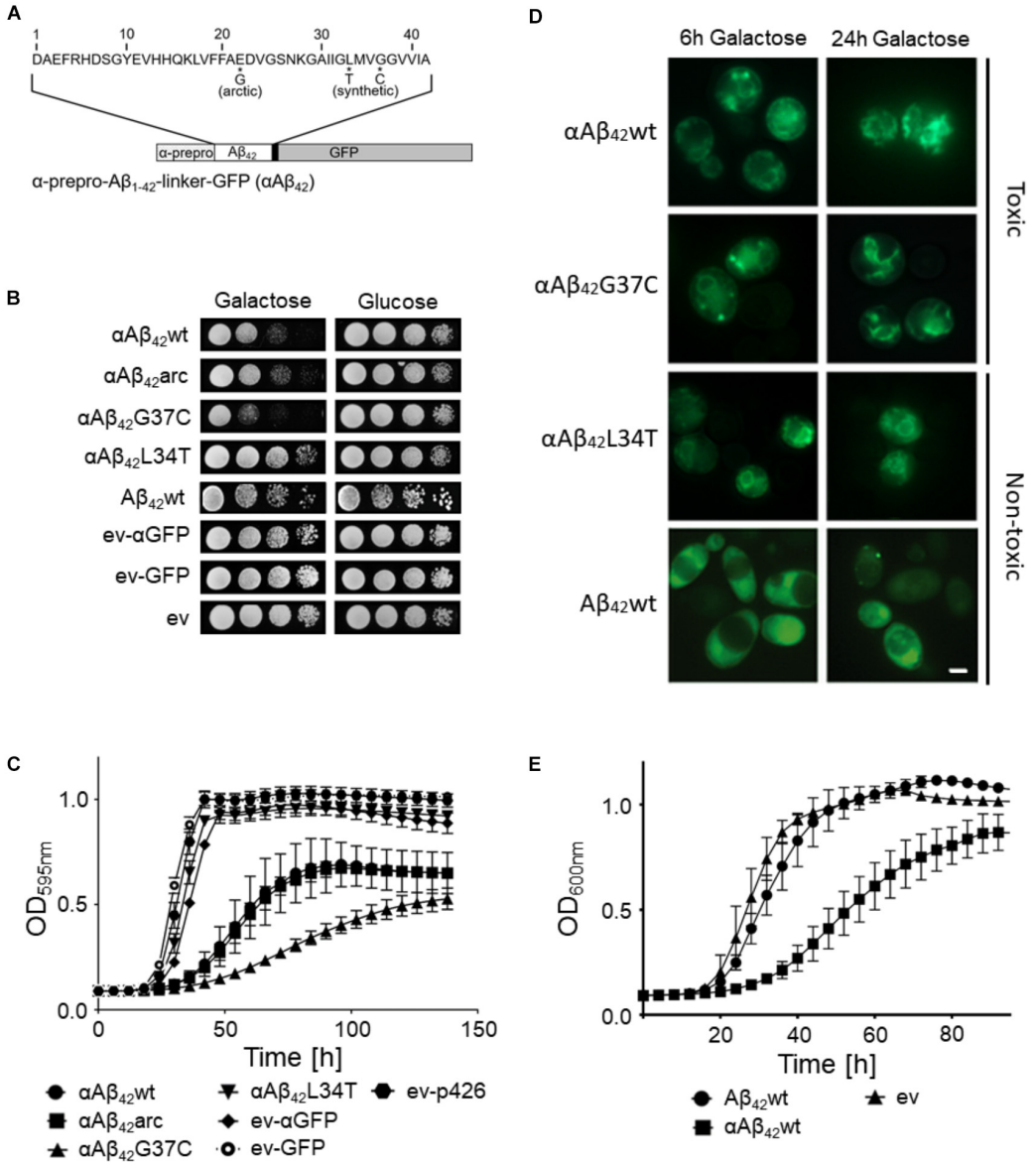

FIGURE 1 | Toxicity profiles of wild-type or mutant αAβ$_{42}$ in the haploid *Saccharomyces cerevisiae* strains BY4741. **(A)** Schematic representation of the α-prepro-Aβ$_{42}$-linker-GFP construct with indication of the mutants used in this study. **(B)** Spot assays under inducing (galactose) and repressing (glucose) conditions and **(C)** growth profiles under inducing conditions of the BY4741 wild-type strain transformed with constructs allowing for expression of αAβ$_{42}$wt, αAβ$_{42}$arc, αAβ$_{42}$G37C, αAβ$_{42}$L34T, Aβ$_{42}$wt and control vectors (ev-αGFP, ev-GFP, ev) as indicated. Error bars in the growth profiles represent the standard deviation of at least four independent transformants. **(D)** Fluorescence microscopy pictures show localization of α-prepro fused Aβ$_{42}$ mutants to the ER 6 and 24 h after induction on galactose-containing medium. 24 h after induction of gene expression the toxic αAβ$_{42}$ isoforms show a more "patchy" pattern while the non-toxic αAβ$_{42}$L34T still localizes at the ER. The Aβ$_{42}$wt construct lacking the α-prepro sequence is seen in the cytoplasm. The scale bar represents 2 μm. **(E)** Growth profiles of the BY4741 wild-type strain transformed with an empty vector (ev) or constructs allowing for expression of αAβ$_{42}$wt and Aβ$_{42}$wt.

slower than those transformed with ev-GFP or ev (**Figures 1B,C** and **Supplementary Figure S1A**), both spot assays and growth analysis in liquid medium confirmed that wild-type or mutant αAβ$_{42}$ instigated a significantly higher level of toxicity that was similar in the BY4741 and the BY4742 strains (**Figures 1B,C** and **Supplementary Figure S1**). The synthetic αAβ$_{42}$G37C mutant was the most toxic followed by αAβ$_{42}$wt and αAβ$_{42}$arc. The synthetic αAβ$_{42}$L34T mutant, on the other hand, did not yield a toxic phenotype and these transformants grew similar as those expressing ev-αGFP, thereby confirming previously reported data (Vignaud et al., 2013).

Fluorescence microscopy showed that all αAβ$_{42}$ constructs clearly stained the perinuclear ER and to a lesser extent the cortical ER and that particularly the cells expressing the toxic

$\alpha A\beta_{42}$ forms often displayed ER-associated foci and filamentous structures (**Figure 1D**). These were previously believed to be vesicles (D'Angelo et al., 2013), but recent studies suggests that these may as well-represent ER-aggregates or clustering of ER membranes, both indicative for ER stress (Varadarajan et al., 2012, 2013; Vevea et al., 2015). In contrast, when the $A\beta_{42}$wt was expressed from a construct that lacks the α-prepro sequence, the GFP fusion was mainly found to be distributed in the cytoplasm though some cells presented foci after prolonged induction (**Figure 1D**). Despite of these foci, the expression of the $A\beta_{42}$wt construct without the α-prepro sequence only triggered a small growth retardation (**Figures 1B,E**). This nicely demonstrates that the processing in the ER/Golgi system is required to unleash the full toxic capacity of $\alpha A\beta_{42}$.

Retention of $\alpha A\beta_{42}$ in the ER Diminishes Its Toxicity

Previously, we reported that the processing of the $\alpha A\beta_{42}$-linker-GFP fusion constructs in the ER/Golgi system yields three distinct isoforms when performing Western blot analysis, i.e., the α-prepro precursor (41 kDa), the glycosylated precursor (50 kDa), and the matured $A\beta_{42}$-linker-GFP form (34 kDa) (D'Angelo et al., 2013; Vignaud et al., 2013). Given that the latter is shuttled into the secretory pathway, we wondered if retention of the $\alpha A\beta_{42}$-linker-GFP fusion in the endoplasmic reticulum (ER) would affect its toxic capacity. To this end, we introduced a HDEL retention signal at the C-terminal end of the construct. The yeast HDEL sequence is equivalent to the mammalian KDEL retention signal that shuttles the KDEL containing proteins back to the ER lumen (Dean and Pelham, 1990; Lewis and Pelham, 1990; Ruan et al., 2017). Consistently, microscopic analysis demonstrated that while both $\alpha A\beta_{42}$G37C and $\alpha A\beta_{42}$G37C-HDEL are equally present at the perinuclear ER, the latter accumulated more in the peripheral cortical ER (**Figure 2A**). Also, Western blot analysis showed that in case of expression of $\alpha A\beta_{42}$G37C-HDEL, both the non-processed $\alpha A\beta_{42}$G37C precursor as well as the glycosylated version accumulated, while the fully processed $A\beta_{42}$G37C was significantly reduced (**Figure 2B**). Next, a growth analysis was performed. This revealed that the strain expressing $\alpha A\beta_{42}$G37C-HDEL construct grew much better than that with $\alpha A\beta_{42}$G37C, thereby displaying a level of toxicity comparable to a strain with the $\alpha A\beta_{42}$arc mutant (**Figure 2C**).

In order to confirm these results with a different approach, we expressed $\alpha A\beta_{42}$wt, $\alpha A\beta_{42}$arc, as well as the super-toxic $\alpha A\beta_{42}$G37C mutant in a BY4741 strain deleted for *ERV29*, which encodes a transmembrane factor involved in COP-II dependent vesicle formation and in trafficking of the α-prepro factor from the ER to the Golgi apparatus (Belden and Barlowe, 2001). Upon deletion of *ERV29*, $\alpha A\beta_{42}$ gets stuck in the ER and cannot transit to the Golgi. Strikingly, cytotoxicity of all tested mutants was indeed significantly diminished in this *erv29*Δ strain and even the super-toxic $\alpha A\beta_{42}$G37C mutant almost completely lost its toxic power (**Figures 2D,E**). Thus, the data above confirm that $\alpha A\beta_{42}$ needs to be fully processed and exit the ER in order to gain its full toxic potential.

$\alpha A\beta_{42}$ Affects Mitochondrial Functioning

Since $\alpha A\beta_{42}$ confers toxicity by entering the secretory pathway, we wanted to know more about the targets and processes being affected. Therefore, we first focused on mitochondria given that previous studies have associated $A\beta_{42}$ to mitochondrial dysfunction in yeast (Chen and Petranovic, 2015; Chen et al., 2017; Hu et al., 2018). To this end, we co-expressed $\alpha A\beta_{42}$wt, $\alpha A\beta_{42}$arc, $\alpha A\beta_{42}$G37C, $\alpha A\beta_{42}$L34T or the ev-αGFP together with a mCherry labeled mitochondrial marker Cox4 in wild-type cells. As illustrated in **Figure 3A**, this suggests a toxicity dependent co-localization since $\alpha A\beta_{42}$wt and even more $\alpha A\beta_{42}$G37C seem to partially co-localize with mitochondria. We then performed a DHE staining to estimate the ROS levels as marker for mitochondrial dysfunction and a PI staining to monitor the amount of cells with disrupted plasma membranes as marker for cell demise (**Figures 3B,C** and **Supplementary Figure S2**). As expected, and consistent with previously reported data (Chen and Petranovic, 2015; Chen et al., 2017), also these aspects correlated to the observed $\alpha A\beta_{42}$ instigated toxicity. Although our data on co-localization suggest that $\alpha A\beta_{42}$ may directly interfere with mitochondrial functioning, we cannot exclude that these effects on mitochondrial function or morphology are indirect, for instance due alterations in ER-mitochondrial communication via ERMES contact sites.

Identification of Additional Processes Underlying $\alpha A\beta_{42}$ Toxicity

To decipher which additional processes sustain the $\alpha A\beta_{42}$ toxicity, we performed two unbiased genetic screens. In a first screening setup, we aimed to identify alleviators of $A\beta_{42}$G37C toxicity. Therefore, we transformed a pooled Euroscarf knock-out (KO) library with the $\alpha A\beta_{42}$G37C-linker-GFP construct and looked for transformants that grew similar as the empty vector control. Out of 90,000 transformants obtained when plated on repressive glucose containing medium, only 465 were able to form visible colonies after 72 h on galactose-containing medium where the expression of the super-toxic $A\beta_{42}$ mutant is induced. Each colony was then plated on SD medium supplemented with casamino acids to manually confirm the suppressive effect on $\alpha A\beta_{42}$ toxicity. Of the 465 initial clones, 268 were still able to grow. Finally, we characterized each KO strain by sequencing the PCR amplicon of its bar-code region. This led us to identify 113 different KO strains. In the second screening setup, we performed an unbiased SGA analysis with the full gene knock-out library using either $\alpha A\beta_{42}$wt, the super-toxic $\alpha A\beta_{42}$G37C mutant and the ev-GFP control. The additional use of the empty vector control and $\alpha A\beta_{42}$wt, which displays a more moderate toxicity phenotype, allowed for more complete results since not only suppressors but also toxicity aggravators could be scored. With this SGA screen, we identified 87 additional KO strains that modulated $\alpha A\beta_{42}$ toxicity, one of which contains a deletion in the overlapping genes *INP52/RRT16*. Finally, the 200 KO strains that were identified by either one of the screening procedures (**Table 3** and **Supplementary Table S1**) were also transformed individually with a construct allowing for the expression of $\alpha A\beta_{42}$arc, which has an intermediate toxicity similar to that

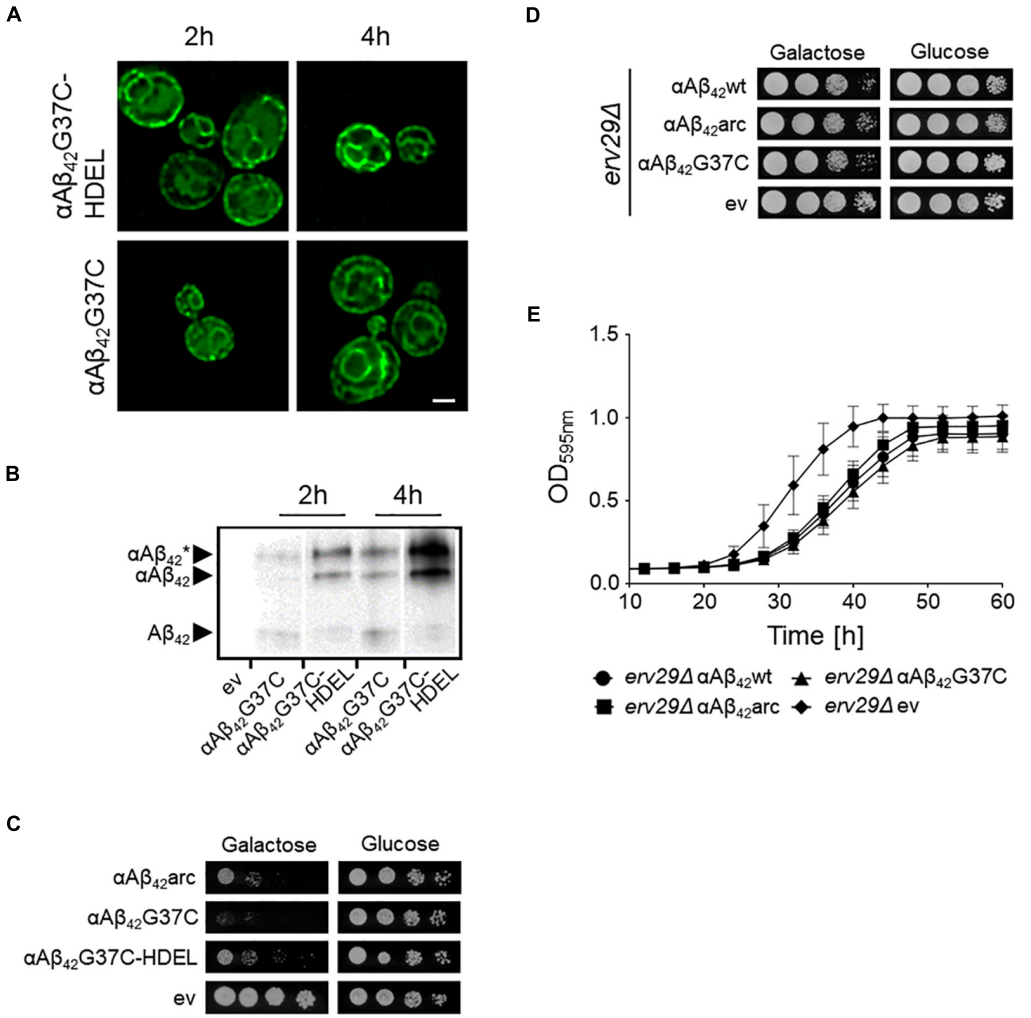

FIGURE 2 | Retention of $\alpha A\beta_{42}$ in the ER and the consequence for toxicity. **(A)** Fluorescence microscopy pictures showing $\alpha A\beta_{42}$G37C and $\alpha A\beta_{42}$G37C-HDEL localization at the perinuclear and cortical ER. Scale bar represents 2 μm. **(B)** Western blot analysis of total protein extracts obtained from cells expressing either $\alpha A\beta_{42}$G37C and $\alpha A\beta_{42}$G37C-HDEL. The different processing isoforms are indicated, i.e., $\alpha A\beta^*_{42}$ indicates glycosylated $\alpha A\beta_{42}$, $\alpha A\beta_{42}$ indicates un-glycosylated $\alpha A\beta_{42}$ and $A\beta_{42}$ indicates fully processed form where the α-prepro sequence is cleaved off. Spot assays under inductive (galactose) and repressive (glucose) conditions of wild-type **(C)** or *erv29*Δ **(D)** cells transformed with the empty vector (ev) or constructs allowing for expression of $\alpha A\beta_{42}$wt, $\alpha A\beta_{42}$arc, $\alpha A\beta_{42}$G37C, or $\alpha A\beta_{42}$G37C-HDEL as indicated. **(E)** Growth profiles of *erv29*Δ transformed with the empty vector (ev) or constructs allowing for expression of $\alpha A\beta_{42}$wt, $\alpha A\beta_{42}$arc, or $\alpha A\beta_{42}$G37C when grown on galactose-containing medium.

of $\alpha A\beta_{42}$wt and thus is again ideal to provide confirmation of both aggravators and suppressors of toxicity (D'Angelo et al., 2013). This provided an independent confirmation that all the KO strains selected in one of the two genetic screens are indeed involved in modulating $\alpha A\beta_{42}$arc toxicity. For each of the KO strains, the cell density under galactose inducing conditions was monitored allowing to rank KO strains from 0 to 5 depending on the growth capacity in comparison to the wild-type strain transformed $\alpha A\beta_{42}$arc. For 29 KO strains, growth was improved strongly (scored as 5), for 18 KO strains growth was clearly improved (scored as 4) and for 129 KO strains growth was only slightly better (scored as 3). On the other hand, we also identified 2 KO strains in which $\alpha A\beta_{42}$arc toxicity was strongly enhanced (scored as "0") and 17 KO strains that enhanced $\alpha A\beta_{42}$arc toxicity moderately (scored as 1) or weakly (scored as 2) (**Table 3** and **Supplementary Table S1**). Next, a gene ontology (GO) analysis using the SGD Gene Ontology Slim Mapper[1] allowed to sort the KO strains into functional categories depending on the gene deleted (**Table 3**). These included, amongst others, cytoskeleton organization and endocytosis, protein sorting and trafficking, protein ubiquitination, plasma membrane transport, cell cycle, translation, and transcription.

Interestingly, among the many KO strains that alleviated $\alpha A\beta_{42}$arc toxicity we found not only the strain deleted for *ERV29*, which is in line with the data described above, but also strains lacking other genes that impact on ER/Golgi functioning

[1]https://www.yeastgenome.org/cgi-bin/GO/goSlimMapper.pl

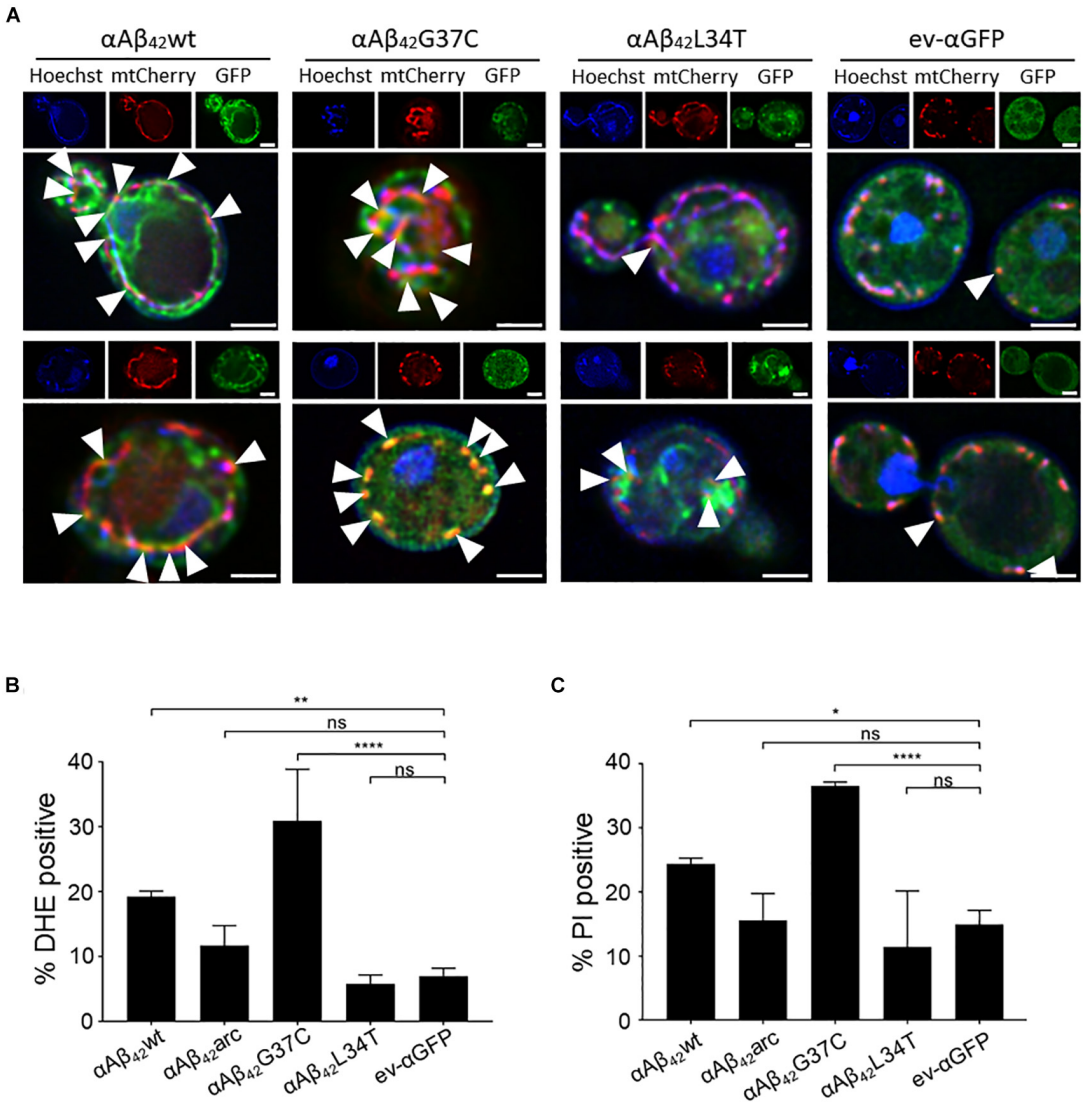

FIGURE 3 | $\alpha A\beta_{42}$ induces mitochondrial dysfunction and cell demise. **(A)** Fluorescence microscopy pictures suggesting partial co-localization of toxic $\alpha A\beta_{42}$ but not of the non-toxic $\alpha A\beta_{42}$L34T nor of the αGFP control (green) with mitochondria (red) in wild-type cells. Hoechst staining (blue) shows mitochondrial as well as nuclear DNA. The white arrowheads indicate sites of co-localization between $\alpha A\beta_{42}$ and mitochondria. Two single cells shown per strain. Scale bars represent 2 μm. Percentage of wild-type yeast cells expressing wild-type or mutant $\alpha A\beta_{42}$ and a control stained with DHE as a marker for ROS-formation **(B)** or PI as a marker for plasma membrane integrity **(C)**. $^{*}P \leq 0.05$; $^{**}P \leq 0.01$; $^{****}P \leq 0.0001$; $^{ns}P > 0.05$.

and traffic, such as the *SPC2* encoded subunit of the peptidase complex, which cleaves the signal sequence from proteins targeted to the ER, *EMP24*, which encodes a component of the p24 complex that mediates ER-to-Golgi transport of GPI anchored proteins, or *ARF2* and *YPT31*, which both encode GTPases required for intra-Golgi traffic. Also found were several strains lacking genes encoding mitochondrial functions and this included *AIF1* that codes for the mitochondrial cell death effector, indicative that $\alpha A\beta_{42}$ actively induces programmed cell death pathways. Furthermore, the fact that we retrieved the KO strains for *ATG1*, *ATG2,* and *ATG20* suggests that $\alpha A\beta_{42}$ may overstimulate the autophagy and the cytoplasm-to-vacuole targeting pathways (Kim and Klionsky, 2000; Nice et al., 2002). Finally, it was recently shown by transcriptome analysis that $A\beta_{42}$ impacts on lipid metabolism with *INO1* being most significantly upregulated (Chen et al., 2017). We found the KO strain lacking *ITC1* to reduce $\alpha A\beta_{42}$ toxicity. *ITC1* encodes a subunit of ATP-dependent Isw2p-Itc1p chromatin remodeling complex that is required for repression of *INO1*. In addition, also KO strains lacking genes involved sphingolipid and ceramide metabolism were retrieved, i.e., *FAA1*, *SUR1*, *YDC1*. Overall, these data confirm that the noxious effect of $\alpha A\beta_{42}$ is associated to changes in lipid metabolism.

The KO strains that aggravated $\alpha A\beta_{42}$ toxicity were often missing functions associated to maintenance and organization of the actin cytoskeleton, endocytosis and the multivesicular

TABLE 3 | $\alpha A\beta_{42}$ toxicity modifiers.

GO term	Enhancers	Suppressors
Biological process unknown	**FMP41** (2), **MTC3** (2), YBR113W (2), YHL005C (2), YJL169W (2)	GL081W (3), ICY1 (3), IRC10 (3), MRX11 (3), NBA1 (3), NRP1 (3), PHM7 (3), PRM9 (3), RRT16 (3), TDA8 (3), URN1 (3), YBR209W (3), YBR284W (3), YCR085W (3), YCR099C (3), YDR042C (3), YER067C-A (3), YER186C (3), YGL101W (3), YGR259C (3), YIL014C-A (3), YKL066W (3), YL043W (3), YLR042C (3), YLR279W (3), **YLR283W** (3), YML096W (3), YML119W (3), YMR102C (3), YMR153C-A (3), YMR160W (3), YMR178W (3), YMR244W (3), YMR316C-A (3), YMR317W (3), YNL146W (3), YOR263C (3), YPL257W (3), YGL109W (4), YJL007C (4), YMR114C (4), YNL338W (4), YNR071C (4), YGL072C (5), YLR149C (5), YML084W (5), YMR103C (5), YOR296W (5), YPL247C (5)
Cell cycle	**END3** (2), **RIM8** (2), **CCR4** (2)	**CLN1** (3), **DIA2** (3), **FYV5** (3), **GAS2** (3), **MAM1** (3), **NFI1** (3), **PCL1** (3), **PEA2** (3), **REC114** (3), **PRM3** (3), **SMK1** (3), **SRC1** (3), **SSO2** (3), **SSP1** (3), **TEC1** (3), **TEP1** (3), **TOF1** (3), **YOR338W** (3), **BDF2** (4), **ITC1** (4), **REI1** (4), **XRN1** (4), **ADA2** (5), **CLB3** (5), **CSM4** (5), **STE24** (5), **YHP1** (5), **ZDS1** (5)
Cell morphology	**END3** (2)	**GAS2** (3), **GPD2** (3), **PEA2** (3), **SMK1** (3), **SSP1** (3), **TEP1** (3), **REI1** (4)
Cytoskeleton	SAC6 (0), **BEM2** (2), **END3** (2), **RVS167** (0), **SLA1** (2) TDA2 (2)	**ABP1** (3), **PCL1** (3), **PEA2** (3), **SLM2** (3), **WHI2** (3), **CLB3** (5), **PFD1** (5)
DNA	**CCR4** (2), **SLX8** (2)	**ADA2** (5), **CSM4** (5), **DIA2** (3), HCS1 (3), **RAD34** (3), **REC114** (3), **RPB9** (3), **SLX5** (3), **TEC1** (3), **TOF1** (3)
Mitochondria	**MTC3** (2), **FMP41** (2), **RTG1** (2), **SAM37** (2)	**HEM25** (3), MRX5 (3), **AIM25** (3), **YLR283W** (3), **GUF1** (3), **AIF1** (3), **ODC1** (3), **MDL2** (3), **YME1** (3), **SUE1** (3), **PKP1** (4), **FMP25** (4), **RSM25** (5), **FMP30** (5)
Metabolism	**TDA9** (2)	ALD2 (3), ALD3 (3), CPA1 (3), **FAA1** (3), FAA3 (3), FAU1 (3), **GPD2** (3), LEU4 (3), NMA1 (3), SNO2 (3), SUR1 (3), YDC1 (3), IGD1 (4), **FMP30** (5), HIS1 (5), **PSK2** (5), SPE2 (5)
Organelle organization	**SAM37** (2), **RIM8** (2)	**ABP1** (3), **AIM25** (3), **ATG1** (3), ATG2 (3), **ATG20** (3), DID2 (3), **DJP1** (3), IWR1 (3), **MAM1** (3), **NGR1** (3), **PEA2** (3), **PEX6** (3), **PRM3** (3), **REC114** (3), SPC2 (3), **SRC1** (3), **SSO2** (3)**TOF1** (3), VPS68 (3), **WHI2** (3), **YME1** (3), **BDF2** (4), **FMP25** (4), **ADA2** (5), **CLB3** (5), **CSM4** (5) **SCD6** (5)
Other	**BEM2** (2), **END3** (2), **RIM8** (2), **RTG1** (2)	ADH6 (3), APE2 (3), ARF2 (3), **DIA2** (3), FDO1 (3), **FYV5** (3), IGO2 (3), **ODC1** (3), OXP1 (3), **PEX6** (3), PML39 (3), **SLM2** (3), **GAS2** (3), **SMK1** (3), **SSO2** (3), **SSP1** (3), **SUE1** (3), **TEC1** (3), **TEP1** (3), TVP18 (3), YML082W (3), **YOR338W** (3), ECM4 (4), PDE2 (4), YGR111W (4)
Protein modification	**SNF7** (1), HPM1 (2), **PKR1** (2), **RIM8** (2), **SAM37** (2), **SLA1** (2), **SLX8** (2), **UMP1** (2), **VPS24** (2)	**ABP1** (3), **ATG1** (3), **CLN1** (3), CPS1 (3), CUL3 (3), CUR1 (3), **DIA2** (3), **NFI1** (3), **HRT3** (3), **MAM1** (3), **PCL1** (3), **SLX5** (3), **SMK1** (3), SPC2 (3), **SSP1** (3), TUL1 (3), **YME1** (3), **FMP25** (4), **PKP1** (4), **XRN1** (4), **ADA2** (5), **CLB3** (5), **PFD1** (5), **PSK2** (5), **STE24** (5)
RNA	**CCR4** (2)	DEG1 (3), HIT1 (4), NGL2 (3), **RPB4** (3), RPS8A (3), **XRN1** (4), CBC2 (5), MSL1 (5), SNT309 (5), **TSR3** (5)
Stress response	**SNF7** (1), **PKR1** (2), **PMP3** (2), **RTG1** (2), **RVS167** (0), **SLX8** (2), **UMP1** (2)	**AIF1** (3), **AIM25** (3), CUR1 (3), **FYV5** (3), HYR1 (3), **MDL2** (3), MIG1 (3), **PEA2** (3), **RAD34** (3), **RPB4** (3), **RPB9** (3), **SLX5** (3), SMF3 (3), **TOF1** (3), YCR102C (3), **ITC1** (4), TRK1 (5), **WHI2** (3), **ADA2 (5), YAR1 (5)**
Transcription	**CCR4** (2), **RTG1** (2), **TDA9** (2)	CAF120 (3), FUI1 (3), GAT2 (3), **ITC1** (4), MIG1 (3), **RPB4** (3), **RPB9** (3), **TEC1** (3), **YOR338W** (3), FZF1 (4), STP1 (4), **XRN1** (4), **ADA2** (5), MBF1 (5), **PFD1** (5), **YHP1** (5)
Translation	RPS7A (2)	**GUF1** (3), **NGR1** (3), **RPB4** (3), RPS7B (3), RPS8A (3), HIT1 (4), **REI1** (4), **PSK2** (5), RPL2B (5), **RSM25** (5), **SCD6** (5), **TSR3** (5), **YAR1 (5)**
Transport (not vesicular)	**SNF7** (1), **PMP3** (2), **SAM37** (2), VPS24 (2)	ATO3 (3), **DJP1** (3), **FAA1** (3), FUI1 (3), GFD1 (5), **HEM25** (3), IWR1 (3), **MDL2** (3), MSN5 (3), NRT1 (3), **PEX6** (3), PUT4 (3), **RPB4** (3), SMF3 (3), **YME1** (3), YOL163W (3), FZF1 (4), **REI1** (4),**YAR1 (5)**, **ZDS1** (5)
Vesicles/trafficking	**RVS167** (0), **SNF7** (1), **END3 (2), RIM8** (2), **SLA1** (2), **VPS24** (2)	**ATG20** (3), DID2 (3), EMP24 (3), **PRM3** (3), **SLM2** (3), **SSO2** (3), VPS68 (3), **WHI2** (3), YPT31 (3), SLM6 (4), ERV29 (5)

Enhancers and suppressors of the $\alpha A\beta_{42}$ instigated toxicity are shown. Genes are sorted according to the Gene Ontology (GO) terms. Category "Mitochondria" was manually added according to GO terms list. Genes that occur in more than 1 GO-term category are in bold. The numbers between brackets refer to the growth scores ranging from 0 (worst growth) to 5 (best growth). See main text for details.

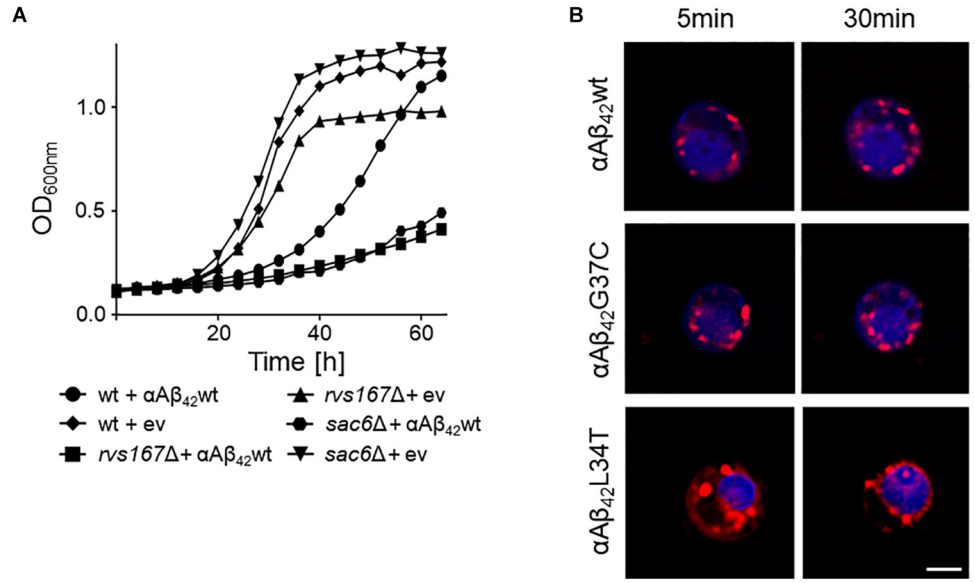

FIGURE 4 | Interference of $\alpha A\beta_{42}$ with endocytosis. **(A)** Growth profiles of wild-type cells and *rvs167*Δ or *sac6*Δ cells transformed with the empty vector (ev) or a construct allowing for expression of $\alpha A\beta_{42}$wt when grown on galactose-containing medium. **(B)** Fluorescence microscopy pictures of strains expressing the toxic $\alpha A\beta_{42}$wt and $\alpha A\beta_{42}$G37C or the non-toxic $\alpha A\beta_{42}$L34T stained with the endocytosis tracker FM4-64 (red) and CMAC (blue), a dye to stain the vacuolar lumen. The scale bar represents 2 μm.

body (MVB) pathway. The two strains with the strongest enhanced toxicity were those carrying a deletion of *SAC6* or *RVS167*. Sac6 is an actin-bundling protein that is required for endocytosis (Penalver et al., 1997; Gheorghe et al., 2008). Rvs167 is a homolog of mammalian amphiphysin that interacts with actin as well and that functions in the internalization step of endocytosis (Lombardi and Riezman, 2001). As illustrated for the expression of $\alpha A\beta_{42}$wt, we indeed observed a similar severe growth phenotype in both the *sac6*Δ and *rvs167*Δ mutants as compared to the isogenic wild-type strain (**Figure 4A**). To further confirm the link between endocytosis and $\alpha A\beta_{42}$ toxicity, we also monitored the uptake of the endocytosis tracker FM4-64 by wild-type cells expressing either the toxic $\alpha A\beta_{42}$wt and $\alpha A\beta_{42}$G37C and non-toxic $\alpha A\beta_{42}$L34T isoforms after 4 h induction on galactose-containing medium. As shown, FM4-64 already stained the vacuolar membrane within 30 min in cells expressing the non-toxic construct while no, or only a minimal staining of the vacuolar membrane was observed in cells expressing the toxic $\alpha A\beta_{42}$ species, even not after 60 min of incubation (**Figure 4B**). This demonstrates that the latter have a direct impact on the endocytic process.

$\alpha A\beta_{42}$ Enhances the Occurrence of Plasma Membrane Lesions and Formation of Lipid Droplets

Closely connected to endocytosis, we noticed that our screening retrieved some ESCRT components, which function in the MVB pathway that is required for the turnover of plasma membrane proteins and lipids. The first step in MVB formation is the binding of ESCRT-0 (Hse1 and Vps27) and ESCRT-I (involving Vps28, Mvb12, Srn2, and Stp22) to ubiquitinated MVB cargoes. Next, the ESCRT-II complex (involving Vps25, Vps36, and Snf8) mediates the recruitment of ESCRT-III accessory factors (Bro1 and Doa4), which in turn loads general ESCRT-III factors (Vps20, Snf7, Did4, Chm7, Ist1, and Vps24) to direct the continued sorting of cargoes into invaginating vesicles during MVB formation. ESCRT-III dissociation factors (Vps4, Vps60, Did2, and Vta1) mediate the release and recycling of all involved factors (Hurley, 2010; Babst, 2011). All the 21 corresponding genes are not essential and could therefore be tested for their implications in $\alpha A\beta_{42}$ toxicity. After transformation of the corresponding KO strains with either $\alpha A\beta_{42}$wt, $\alpha A\beta_{42}$G37C or the ev-αGFP control construct, we evaluated the impact of the deletions on $\alpha A\beta_{42}$ toxicity through spot assays. This revealed that for several components of the MVB pathway their deletion significantly aggravated $\alpha A\beta_{42}$ toxicity. This included the ESCRTIII components Did4, the ESCRTIII accessory components Bro1 and Doa4 as well as the ESCRTIII dissociation mediator Vps4 (**Supplementary Figures S3, S4**). Recent studies in mammalian cells have demonstrated that besides its role in the MVB pathway, ESCRT plays key roles in a variety of other processes, including membrane lesion repair (Jimenez et al., 2014; Sundquist and Ullman, 2015; Campsteijn et al., 2016; Denais et al., 2016; Raab et al., 2016). It is well-established that $A\beta_{42}$ can introduce membrane lesions and different non-excluding mechanisms were proposed, including membrane lipid interaction, alterations in membrane fluidity, pore formation, or lipid oxidation (Eckert et al., 2000; Muller et al., 2001; Ambroggio et al., 2005; Rauk, 2008; Axelsen et al., 2011; Viola and Klein, 2015). We speculated that $\alpha A\beta_{42}$ would also trigger membrane lesions in our yeast system. To test this, we analyzed

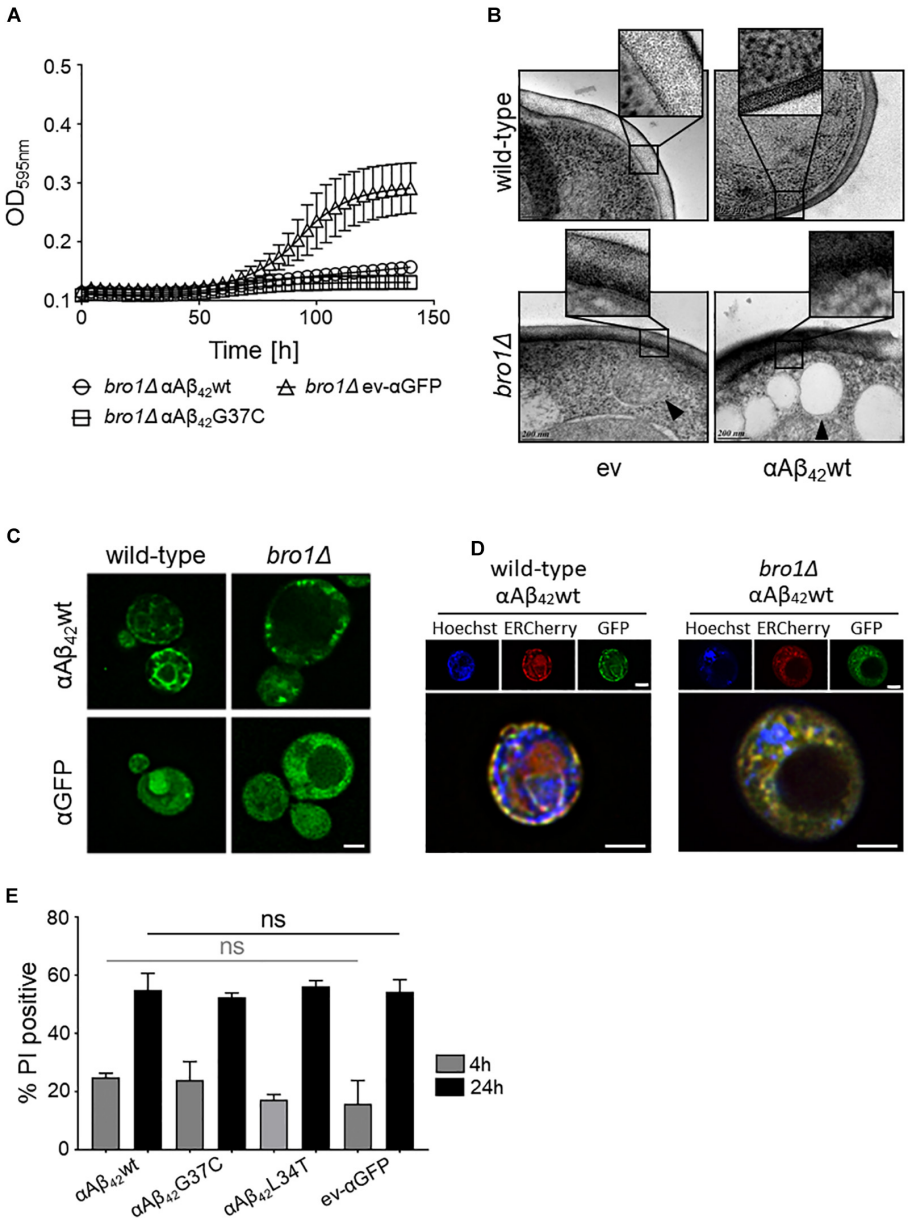

FIGURE 5 | The role of Bro1 for membrane lesion repair. **(A)** Growth profile on galactose-containing medium of a strain deleted for the ESCRT-III accessory factor *BRO1* transformed with an empty vector (ev-αGFP) or constructs allowing for expression of $\alpha A\beta_{42}$wt or $\alpha A\beta_{42}$G37C. Cryo-EM pictures **(B)** and fluorescence microscopy pictures **(C)** of wild-type and *bro1*Δ cells transformed with an empty vector (ev) or expressing $\alpha A\beta_{42}$wt and grown for 6 h on galactose-containing medium. The indents in panel **(B)** zoom in on the plasma membrane and cell wall. The black arrowhead in **(B)** indicates a lipid droplet. Scale bars for cryo-EM pictures represent 200 nm. **(D)** BY4742 wild-type and a *bro1*Δ strains transformed with a plasmids carrying $\alpha A\beta_{42}$wt and additionally a plasmid allowing the expression of $Kar2_{(1-135)}$-mCherry-HDEL (ERCherry), a marker for the ER. DNA was stained with Hoechst. Cells were grown in medium allowing for gene expression for 6 h prior to microscopy. Scale bars for fluorescence pictures represent 2 μm. **(E)** PI staining of cells deleted for *BRO1* transformed with constructs allowing for expression of $\alpha A\beta_{42}$wt, $\alpha A\beta_{42}$L34T, $\alpha A\beta_{42}$G37C, or αGFP after 4 or 24 h growth on galactose-containing medium. Error bars represent standard deviations of at least four independent transformants.

the plasma membrane integrity of wild-type and *bro1*Δ cells by cryo-EM. We chose the *bro1*Δ strain because here $\alpha A\beta_{42}$wt and $\alpha A\beta_{42}$G37C was almost lethal (**Figure 5A**) and because Bro1 is the yeast ortholog of human Alix, a proposed biomarker for AD (Sun et al., 2015). Consistent with our hypothesis, the cryo-EM study showed that the plasma membrane of *bro1*Δ cells expressing $\alpha A\beta_{42}$wt seemed heavily corrugated while the *bro1*Δ cells transformed with empty vector displayed a more modest phenotype. In the wild-type strain, the plasma membrane remained ostensibly smooth even upon expression of $\alpha A\beta_{42}$wt (**Figure 5B**). However, although we did not quantify, the observed membrane corrugating effects of specifically the *bro1*Δ

strain expressing αAβ$_{42}$wt are strikingly obvious. Moreover, when compared to the wild-type cells, the ER morphology in the *bro1*Δ mutant was completely different and appeared to be deteriorated. Indeed, only a minimal perinuclear and cortical ER was detected and the cells displayed the αAβ$_{42}$-linker-GFP fusion mostly in filamentous structures and foci (**Figures 5C,D**). Thus, expression of αAβ$_{42}$wt seems to dramatically affect all membranous structures evidencing that Bro1, and by extension the ESCRT system, is absolutely required for the repair of membrane lesions induced by αAβ$_{42}$. In line with this essential requirement of ESCRT, we observed that while still seeing a tendency of increased PI uptake after 4 h induction for those *bro1*Δ cells expressing toxic αAβ$_{42}$, a maximal PI uptake in all *bro1*Δ transformants is seen after 24 h, even for those strains expressing the non-toxic αAβ$_{42}$L34T mutant or the ev-αGFP control (**Figure 5E**).

The cryo-EM study also pointed to the formation of cortical vesicle-like structures, which we believe may correspond to lipid droplets. Since previous studies have shown that the formation of lipid droplets denotes an adaptive response to a chronic lipid imbalance (Vevea et al., 2015; Garcia et al., 2018), which is likely to occur in *bro1*Δ strain because of hampered MVB formation and lipid turnover, we decided to perform a Nile Red staining to visualize the droplets. While during the first hours of induction on galactose-containing medium we observed an overall enhanced lipid droplet biogenesis in all *bro1*Δ strains as compared to the respective wild-type strains, the increase was persistent and especially more dense droplets were seen with *bro1*Δ cells expressing αAβ$_{42}$G37C or αAβ$_{42}$wt (**Figure 6A**). This observation confirms previously reported data on an increased lipid droplet load in an Aβ$_{42}$ wild-type strain (Chen et al., 2017).

The perturbation of lipid homeostasis has also been linked to defects in the ER and mitochondria (Vevea et al., 2015), and the latter incited us to monitor the level of ROS in the *bro1*Δ strains. As shown, and comparable to the PI uptake, we found similar high levels of ROS in all strains tested indicative that this is a characteristic mainly associated to the deletion of *BRO1* itself (**Figure 6B**).

DISCUSSION

During the past decades, several studies validated the use of yeast to decipher the pathobiology underlying a variety of human disorders. Especially for degenerative protein folding diseases, like Huntington's, Parkinson's, or Alzheimer's disease, this led to the discovery of processes and molecular pathways contributing to cell demise (Winderickx et al., 2008; Franssens et al., 2010; Swinnen et al., 2011; Porzoor and Macreadie, 2013; Tenreiro et al., 2013, 2017; Chen and Petranovic, 2016; Jiang et al., 2016; Verduyckt et al., 2016; Fruhmann et al., 2017). The insight gained from these studies were not only relevant in the context of disease, but they also clarified fundamental aspects on how a cell manages to maintain proteostasis and the consequences in case this system fails. In this paper, we used a previously reported model to study the repercussions when the APP-derived peptide Aβ$_{42}$ is expressed in yeast (D'Angelo et al., 2013; Vignaud et al., 2013). Though this model makes use of a GFP fusion, the use of the super-toxic Aβ$_{42}$G37C and the non-toxic Aβ$_{42}$L34T mutants clearly demonstrated that the properties of the GFP fusion are dictated by the Aβ$_{42}$ peptide moiety. Furthermore, by comparing constructs with or without an N-terminal fusion with the α-prepro sequence and conditions that retain the α-prepro in the ER, it became obvious that the processing in the ER/Golgi system and the subsequent shuttling into the secretory pathway is essential to unleash the full toxic capacity of the Aβ$_{42}$-linker-GFP fusion. Our data also contradict the argument that the αAβ$_{42}$ instigated toxicity would simply be due to an overload of the ER/Golgi processing system because both wild-type and mutant αAβ$_{42}$ are processed in the same manner (D'Angelo et al., 2013; Vignaud et al., 2013) and no toxicity is seen in case of expression of mutant αAβ$_{42}$L34T.

The use of our yeast model allowed us to confirm some data previously reported. This included the impact of αAβ$_{42}$ on endocytosis (Treusch et al., 2011; D'Angelo et al., 2013), where we now show that strains with a deletion of *SAC6* or *RVS167* display an increased αAβ$_{42}$ toxicity, as well as the impact on mitochondrial functioning (D'Angelo et al., 2013; Chen and Petranovic, 2015; Chen et al., 2017), which we illustrated by co-localization studies and the observation that αAβ$_{42}$ enhances ROS formation. These data are relevant because, indeed, changes in endocytic capacity and mitochondrial dysfunction are typically seen in the pathogenesis of AD and have been observed in other AD models as well (Thomas et al., 2011; Wang et al., 2011; Avetisyan et al., 2016; Schreij et al., 2016; Dixit et al., 2017; Shoshan-Barmatz et al., 2018; Xu et al., 2018). However, the observed partial co-localization of toxic αAβ$_{42}$ with mitochondria may either indicate a direct interaction of the peptide with this organelle or it may simply be a reflection of the interaction between the ER and mitochondria through the membrane contact sites known as ERMES (Kornmann et al., 2009). This aspect needs to be analyzed in more detail. Interestingly, mitochondria associated membranes (MAMs), the mammalian counterpart of ERMES, have already been implicated in AD (Area-Gomez and Schon, 2016; Paillusson et al., 2016). Closely related to the observed mitochondrial dysfunction is our observation that deletion of *AIF1*, encoding a cell death effector, has a protective effect on the αAβ$_{42}$ expressing yeast cells. This suggests that αAβ$_{42}$ may induce an apoptotic-like program in yeast, which fits the finding that neuronal cells die through apoptosis in AD (Ohyagi et al., 2005; Shoshan-Barmatz et al., 2018). Our data also show that particularly the expression of the toxic αAβ$_{42}$ isoforms is linked to the formation of ER-associated foci and filamentous structures. Though we did not study these structures in detail and previously believed these to represent vesicles (D'Angelo et al., 2013), it is well-possible that they may in fact be ER aggregates or clustering of ER membranes, which are both indicative for ER stress (Varadarajan et al., 2012, 2013; Vevea et al., 2015). Also ER stress is associated to AD (Gerakis and Hetz, 2018) and several links between ER stress and mitochondrial dysfunction have been proposed in this neurodegenerative disorder (Costa et al., 2012; Barbero-Camps et al., 2014; Erpapazoglou et al., 2017).

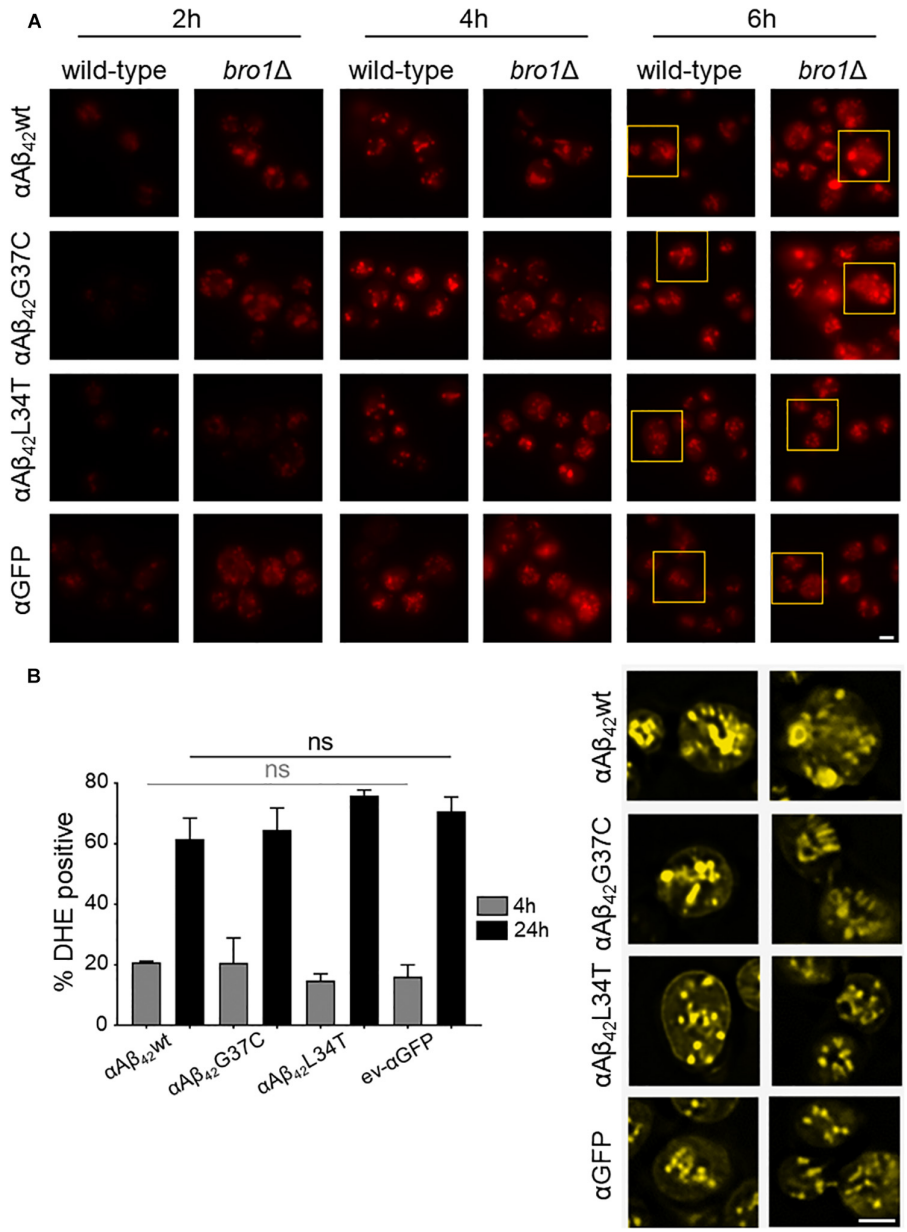

FIGURE 6 | $\alpha A\beta_{42}$ instigated lipid droplet biogenesis. **(A)** Nile Red stainings (top panel), a marker for lipid droplets, of wild-type and the *bro1*Δ cells expressing $\alpha A\beta_{42}$wt, $\alpha A\beta_{42}$G37C, or $\alpha A\beta_{42}$L34T or αGFP after 2, 4, or 6 h growth on galactose-containing medium. The bottom panel (yellow) shows magnifications and deconvolved parts of the top-panel pictures at time point of 6 h. Note that due to deconvolution the picture intensities are enhanced. Scale bars represent 2 μm. **(B)** DHE staining of cells deleted for *BRO1* transformed with constructs allowing for expression of $\alpha A\beta_{42}$wt, $\alpha A\beta_{42}$L34T, $\alpha A\beta_{42}$G37C, or αGFP after 4 or 24 h growth on galactose-containing medium. Error bars represent standard deviations of at least four independent transformants.

One of the most striking observations made in our studies is the role of ESCRT in modulating the $\alpha A\beta_{42}$ toxicity. The ESCRT system functions in the MVB pathway and several studies have linked this role of ESCRT to AD. Neurons of AD transgenic mice were shown to display enlarged MVBs as compared to the neurons of wild-type mice, and ESCRT was demonstrated to modulate intracellular $A\beta_{42}$ accumulation by directing APP to lysosomal degradation and by enhancing $A\beta_{42}$ secretion. In addition, ESCRT components were found associated with amyloid plaques in transgenic mice and to granular structures hippocampal neurons of AD diseased human brain (Yamazaki et al., 2010; Edgar et al., 2015; Willen et al., 2017). However, apart from its function in the MVB pathway, ESCRT is also required for the repair of membrane lesions. Here, both cryo-EM and PI-staining give a strong impression of the presence of such lesions at the plasma membrane of cells lacking the ESCRT component Bro1, probably explaining in part the sick phenotype of the *bro1*Δ mutant. As such, our data strongly

suggest that the role of ESCRT for plasma membrane repair, which so far was only demonstrated in mammalian cells, is evolutionary well-conserved. Interestingly, we found that the disruption of the plasma membrane integrity in the *bro1*Δ strain is dramatically exacerbated upon expression of $\alpha A\beta_{42}$ and that this came along with the deterioration of the ER and an almost lethal phenotype. This is intriguing for several reasons. It demonstrates that when the fully processed $A\beta_{42}$-linker-GFP arrives at the plasma membrane, the peptide further aggravates plasma membrane disruption, which given the observed effect on the ER, might well be involving fusion of secretory vesicles that contain disordered membranes. The fact that our screens retrieved the KO strain lacking *SSO2* as suppressor of $\alpha A\beta_{42}$ toxicity favors the last possibility. Indeed, *SSO2* encodes a plasma membrane t-SNARE that is required for fusion secretory vesicles (Grote et al., 2000). Moreover, the data recapitulate observations made for AD where, as mentioned, $A\beta_{42}$ was shown to introduce membrane lesions via different non-excluding mechanisms, including membrane lipid interaction, alterations in membrane fluidity, pore formation, or lipid oxidation (Eckert et al., 2000; Muller et al., 2001; Ambroggio et al., 2005; Rauk, 2008; Axelsen et al., 2011; Viola and Klein, 2015).

Given the effect of $A\beta_{42}$ on plasma membrane integrity, the presence of this peptide also impacts on the overall cellular lipid homeostasis. In fact, extensive lipid alterations are implicated in the AD disease pathology but it is still a matter of debate whether such alterations are the cause or the consequence of AD (Grosgen et al., 2010; Xiang et al., 2015; El Gaamouch et al., 2016). In yeast, the expression of $A\beta_{42}$ has been linked to a transcriptional upshift of key regulators of lipid metabolism as well as an enhanced formation of lipid droplets (Chen et al., 2017). Our screens with the yeast deletion collection and our Nile Red stainings support the link between $A\beta_{42}$ and lipid metabolism. Intriguingly, a recent study demonstrated lipid droplet formation to be an adaptive response to an acute lipid imbalance in yeast cells. The same study then also showed that the biogenesis of these droplets occurs at ER aggregates (Vevea et al., 2015), which we believe to correspond to the ER-associated foci and filamentous structures seen when yeast cells express toxic forms of $\alpha A\beta_{42}$, as mentioned. Notably, also in transgenic mouse models of AD an enhanced lipid droplet formation is observed (Hamilton et al., 2010; Yang et al., 2014), again underscoring the relevance of the data obtained in yeast.

AUTHOR CONTRIBUTIONS

GF, CM, HV, MV, and NT performed experiments and analyzed data. GF and JW wrote the draft. CDV, CC, and JW contributed conception and design of the studies. CC and JW corrected and edited the draft.

FUNDING

This work was financially supported by the KU Leuven and the FWO Vlaanderen (Project No. G0A6315N). CDV was supported by the Swiss National Science Foundation and the Canton of Fribourg.

ACKNOWLEDGMENTS

We want to thank Joëlle Rosseels, Dorien Vliegen, and Elodie Cougouille for technical and experimental support. We also want to thank Dr. B. Salin and to the Bordeaux Imaging Center (BIC) for performing TEM experiments.

SUPPLEMENTARY MATERIAL

The Supplementary Material for this article can be found online at: https://www.frontiersin.org/articles/10.3389/fnmol.2018.00406/full#supplementary-material

REFERENCES

Abramov, E., Dolev, I., Fogel, H., Ciccotosto, G. D., Ruff, E. (2009). Amyloid-β as a positive endogenous regulator of release probability at hippocampal synapses. *Nat. Neurosci.* 12, 1567–1576. doi: 10.1038/nn.2433

Alexandrov, A. I., Serpionov, G. V., Kushnirov, V. V., and Ter-Avanesyan, M. D. (2016). Wild type huntingtin toxicity in yeast: Implications for the role of amyloid cross-seeding in polyQ diseases. *Prion* 10, 221–227. doi: 10.1080/19336896.2016.1176659

Ambroggio, E. E., Kim, D. H., Separovic, F., Barrow, C. J., Barnham, K. J., Bagatolli, L. A., et al. (2005). Surface behavior and lipid interaction of Alzheimer β-amyloid peptide 1-42: a membrane-disrupting peptide. *Biophys. J.* 88, 2706–2713. doi: 10.1529/biophysj.104.055582

Area-Gomez, E., and Schon, E. A. (2016). Mitochondria-associated ER membranes and Alzheimer disease. *Curr. Opin. Genet. Dev.* 38, 90–96. doi: 10.1016/j.gde.2016.04.006

Avetisyan, A. V., Samokhin, A. N., Alexandrova, I. Y., Zinovkin, R. A., Simonyan, R. A., and Bobkova, N. V. (2016). Mitochondrial dysfunction in neocortex and hippocampus of olfactory bulbectomized mice, a model of Alzheimer's disease. *Biochemistry (Mosc)* 81, 615–623. doi: 10.1134/S0006297916060080

Axelsen, P. H., Komatsu, H., and Murray, I. V. (2011). Oxidative stress and cell membranes in the pathogenesis of Alzheimer's disease. *Physiology (Bethesda)* 26, 54–69. doi: 10.1152/physiol.00024.2010

Babst, M. (2011). MVB vesicle formation: ESCRT-dependent, ESCRT-independent and everything in between. *Curr. Opin. Cell Biol.* 23, 452–457. doi: 10.1016/j.ceb.2011.04.008

Barbero-Camps, E., Fernandez, A., Baulies, A., Martinez, L., Fernandez-Checa, J. C., and Colell, A. (2014). Endoplasmic reticulum stress mediates amyloid beta neurotoxicity via mitochondrial cholesterol trafficking. *Am. J. Pathol.* 184, 2066–2081. doi: 10.1016/j.ajpath.2014.03.014

Belden, W. J., and Barlowe, C. (2001). Role of Erv29p in collecting soluble secretory proteins into ER-derived transport vesicles. *Science* 294, 1528–1531. doi: 10.1126/science.1065224

Benilova, I., Karran, E., and De Strooper, B. (2012). The toxic Aβ oligomer and Alzheimer's disease: an emperor in need of clothes. *Nat. Neurosci.* 15, 349–357. doi: 10.1038/nn.3028

Campsteijn, C., Vietri, M., and Stenmark, H. (2016). Novel ESCRT functions in cell biology: spiraling out of control? *Curr. Opin. Cell Biol.* 41, 1–8. doi: 10.1016/j.ceb.2016.03.008

Chen, X., Bisschops, M. M. M., Agarwal, N. R., Ji, B., Shanmugavel, K. P., and Petranovic, D. (2017). Interplay of energetics and ER stress exacerbates

Alzheimer's amyloid-beta (Abeta) toxicity in yeast. *Front. Mol. Neurosci.* 10:232. doi: 10.3389/fnmol.2017.00232

Chen, X., and Petranovic, D. (2015). Amyloid-β peptide-induced cytotoxicity and mitochondrial dysfunction in yeast. *FEMS Yeast Res.* 15, 1–21. doi: 10.1093/femsyr/fov061

Chen, X., and Petranovic, D. (2016). Role of frameshift ubiquitin B protein in Alzheimer's disease. *Wiley Interdiscip. Rev. Syst. Biol. Med.* 8, 300–313. doi: 10.1002/wsbm.1340

Costa, R. O., Ferreiro, E., Martins, I., Santana, I., Cardoso, S. M., Oliveira, C. R., et al. (2012). Amyloid beta-induced ER stress is enhanced under mitochondrial dysfunction conditions. *Neurobiol. Aging* 33, 824.e825-e816. doi: 10.1016/j.neurobiolaging.2011.04.011

D'Angelo, F., Vignaud, H., Di Martino, J., Salin, B., Devin, A., Cullin, C., et al. (2013). A yeast model for amyloid-beta aggregation exemplifies the role of membrane trafficking and PICALM in cytotoxicity. *Dis. Model Mech.* 6, 206–216. doi: 10.1242/dmm.010108

Dean, N., and Pelham, H. R. (1990). Recycling of proteins from the golgi compartment to the ER in yeast. *J. Cell Biol.* 111, 369–377. doi: 10.1083/jcb.111.2.369

Denais, C. M., Gilbert, R. M., Isermann, P., McGregor, A. L., te Lindert, M., Weigelin, B., et al. (2016). Nuclear envelope rupture and repair during cancer cell migration. *Science (New York, N.Y.)* 352, 353–358. doi: 10.1126/science.aad7297

Dittmar, J. C., Reid, R. J., and Rothstein, R. (2010). ScreenMill: a freely available software suite for growth measurement, analysis and visualization of high-throughput screen data. *BMC Bioinformatics* 11:353. doi: 10.1186/1471-2105-11-353

Dixit, S., Fessel, J. P., and Harrison, F. E. (2017). Mitochondrial dysfunction in the APP/PSEN1 mouse model of Alzheimer's disease and a novel protective role for ascorbate. *Free Radic. Biol. Med.* 112, 515–523. doi: 10.1016/j.freeradbiomed.2017.08.021

Eckert, G. P., Cairns, N. J., Maras, A., Gattaz, W. F., and Muller, W. E. (2000). Cholesterol modulates the membrane-disordering effects of beta-amyloid peptides in the hippocampus: specific changes in Alzheimer's disease. *Dement. Geriatr. Cogn. Disord.* 11, 181–186. doi: 10.1159/000017234

Edgar, J. R., Willen, K., Gouras, G. K., and Futter, C. E. (2015). ESCRTs regulate amyloid precursor protein sorting in multivesicular bodies and intracellular amyloid-beta accumulation. *J. Cell Sci.* 128, 2520–2528. doi: 10.1242/jcs.170233

El Gaamouch, F., Jing, P., Xia, J., and Cai, D. (2016). Alzheimer's disease risk genes and lipid regulators. *J. Alzheimers Dis.* 53, 15–29. doi: 10.3233/JAD-160169

Erpapazoglou, Z., Mouton-Liger, F., and Corti, O. (2017). From dysfunctional endoplasmic reticulum-mitochondria coupling to neurodegeneration. *Neurochem. Int.* 109, 171–183. doi: 10.1016/j.neuint.2017.03.021

Foury, F. (1997). Human genetic diseases: a cross-talk between man and yeast. *Gene* 195, 1–10. doi: 10.1016/S0378-1119(97)00140-6

Franssens, V., Boelen, E., Anandhakumar, J., Vanhelmont, T., Buttner, S., and Winderickx, J. (2010). Yeast unfolds the road map toward alpha-synuclein-induced cell death. *Cell Death Differ.* 17, 746–753. doi: 10.1038/cdd.2009.203

Fruhmann, G., Seynnaeve, D., Zheng, J., Ven, K., Molenberghs, S., Wilms, T., et al. (2017). Yeast buddies helping to unravel the complexity of neurodegenerative disorders. *Mech. Ageing Dev.* 161(Pt B), 288–305. doi: 10.1016/j.mad.2016.05.002

Garcia, E. J., Vevea, J. D., and Pon, L. A. (2018). Lipid droplet autophagy during energy mobilization, lipid homeostasis and protein quality control. *Front. Biosci. (Landmark Ed)* 23, 1552–1563. doi: 10.2741/4660

Gerakis, Y., and Hetz, C. (2018). Emerging roles of ER stress in the etiology and pathogenesis of Alzheimer's disease. *FEBS J.* 285, 995–1011. doi: 10.1111/febs.14332

Gheorghe, D. M., Aghamohammadzadeh, S., Smaczynska-de, R. II, Allwood, E. G., Winder, S. J., and Ayscough, K. R. (2008). Interactions between the yeast SM22 homologue Scp1 and actin demonstrate the importance of actin bundling in endocytosis. *J. Biol. Chem.* 283, 15037–15046. doi: 10.1074/jbc.M710332200

Grosgen, S., Grimm, M. O., Friess, P., and Hartmann, T. (2010). Role of amyloid beta in lipid homeostasis. *Biochim. Biophys. Acta* 1801, 966–974. doi: 10.1016/j.bbalip.2010.05.002

Grote, E., Carr, C. M., and Novick, P. J. (2000). Ordering the final events in yeast exocytosis. *J. Cell Biol.* 151, 439–452. doi: 10.1083/jcb.151.2.439

Hamilton, L. K., Aumont, A., Julien, C., Vadnais, A., Calon, F., and Fernandes, K. J. (2010). Widespread deficits in adult neurogenesis precede plaque and tangle formation in the 3xTg mouse model of Alzheimer's disease. *Eur. J. Neurosci.* 32, 905–920. doi: 10.1111/j.1460-9568.2010.07379.x

Hamza, A., Tammpere, E., Kofoed, M., Keong, C., Chiang, J., Giaever, G., et al. (2015). Complementation of yeast genes with human genes as an experimental platform for functional testing of human genetic variants. *Genetics* 201, 1263–1274. doi: 10.1534/genetics.115.181099

Hu, W., Wang, Z., and Zheng, H. (2018). Mitochondrial accumulation of amyloid beta (Abeta) peptides requires TOMM22 as a main Abeta receptor in yeast. *J. Biol. Chem.* 293, 12681–12689. doi: 10.1074/jbc.RA118.002713

Hurley, J. H. (2010). The ESCRT complexes. *Crit. Rev. Biochem. Mol. Biol.* 45, 463–487. doi: 10.3109/10409238.2010.502516

Ittner, L. M., and Gotz, J. (2011). Amyloid-beta and tau–a toxic pas de deux in Alzheimer's disease. *Nat. Rev. Neurosci.* 12, 65–72. doi: 10.1038/nrn2967

Jackrel, M. E., DeSantis, M. E., Martinez, B. A., Castellano, L. M., Stewart, R. M., Caldwell, K. A., et al. (2014). Potentiated Hsp104 variants antagonize diverse proteotoxic misfolding events. *Cell* 156, 170–182. doi: 10.1016/j.cell.2013.11.047

Jiang, Y., Chadwick, S. R., and Lajoie, P. (2016). Endoplasmic reticulum stress: The cause and solution to Huntington's disease? *Brain Res.* 1648, 650–657. doi: 10.1016/j.brainres.2016.03.034

Jimenez, A. J., Maiuri, P., Lafaurie-Janvore, J., Divoux, S., Piel, M., and Perez, F. (2014). ESCRT machinery is required for plasma membrane repair. *Science* 343:1247136. doi: 10.1126/science.1247136

Kagan, B. L., Jang, H., Capone, R., Teran Arce, F., Ramachandran, S., Lal, R., et al. (2012). Antimicrobial properties of amyloid peptides. *Mol. Pharm.* 9, 708–717. doi: 10.1021/mp200419b

Kim, J., and Klionsky, D. J. (2000). Autophagy, cytoplasm-to-vacuole targeting pathway, and pexophagy in yeast and mammalian cells. *Annu. Rev. Biochem.* 69, 303–342. doi: 10.1146/annurev.biochem.69.1.303

Kornmann, B., Currie, E., Collins, S. R., Schuldiner, M., Nunnari, J., Weissman, J. S., et al. (2009). An ER-mitochondria tethering complex revealed by a synthetic biology screen. *Science* 325, 477–481. doi: 10.1126/science.1175088

Kumar, D. K., Choi, S. H., Washicosky, K. J., Eimer, W. A., Tucker, S., Ghofrani, J., et al. (2016). Amyloid-beta peptide protects against microbial infection in mouse and worm models of Alzheimer's disease. *Sci. Transl. Med.* 8:340ra372. doi: 10.1126/scitranslmed.aaf1059

LaFerla, F. M., Green, K. N., and Oddo, S. (2007). Intracellular amyloid-β in Alzheimer's disease. *Nat. Rev. Neurosci.* 8, 499–509. doi: 10.1038/nrn2168

Lefebvre-Legendre, L., Salin, B., Schaeffer, J., Brethes, D., Dautant, A., Ackerman, S. H., et al. (2005). Failure to assemble the alpha 3 beta 3 subcomplex of the ATP synthase leads to accumulation of the alpha and beta subunits within inclusion bodies and the loss of mitochondrial cristae in *Saccharomyces cerevisiae*. *J. Biol. Chem.* 280, 18386–18392. doi: 10.1074/jbc.M410789200

Lewis, M. J., and Pelham, H. R. B. (1990). A human homologue of the yeast HDEL receptor. *Nature* 348, 162–163. doi: 10.1038/348162a0

Liu, W., Li, L., Ye, H., Chen, H., Shen, W., Zhong, Y., et al. (2017). From *Saccharomyces cerevisiae* to human: the important gene co-expression modules. *Biomed. Rep.* 7, 153–158. doi: 10.3892/br.2017.941

Lombardi, R., and Riezman, H. (2001). Rvs161p and Rvs167p, the two yeast amphiphysin homologs, function together in vivo. *J. Biol. Chem.* 276, 6016–6022. doi: 10.1074/jbc.M008735200

Muller, W. E., Kirsch, C., and Eckert, G. P. (2001). Membrane-disordering effects of beta-amyloid peptides. *Biochem. Soc. Trans.* 29(Pt 4), 617–623. doi: 10.1042/bst0290617

Mumberg, D., Müller, R., and Funk, M. (1994). Regulatable promoters of Saccharomyces cerevisiae: comparison of transcriptional activity and their use for heterologous expression. *Nucleic Acids Res.* 22, 5767–5768. doi: 10.1093/nar/22.25.5767

Nice, D. C., Sato, T. K., Stromhaug, P. E., Emr, S. D., and Klionsky, D. J. (2002). Cooperative binding of the cytoplasm to vacuole targeting pathway proteins, Cvt13 and Cvt20, to phosphatidylinositol 3-phosphate at the pre-autophagosomal structure is required for selective autophagy. *J. Biol. Chem.* 277, 30198–30207. doi: 10.1074/jbc.M204736200

Ohyagi, Y., Asahara, H., Chui, D. H., Tsuruta, Y., Sakae, N., Miyoshi, K., et al. (2005). Intracellular Abeta42 activates p53 promoter: a pathway to

neurodegeneration in Alzheimer's disease. *FASEB J.* 19, 255–257. doi: 10.1096/fj.04-2637fje

Paillusson, S., Stoica, R., Gomez-Suaga, P., Lau, D. H. W., Mueller, S., Miller, T., et al. (2016). There's something wrong with my MAM; the ER-mitochondria axis and neurodegenerative diseases. *Trends Neurosci.* 39, 146–157. doi: 10.1016/j.tins.2016.01.008

Pearson, H. A., and Peers, C. (2006). Physiological roles for amyloid beta peptides. *J. Physiol.* 575, 5–10. doi: 10.1113/jphysiol.2006.111203

Penalver, E., Ojeda, L., Moreno, E., and Lagunas, R. (1997). Role of the cytoskeleton in endocytosis of the yeast maltose transporter. *Yeast* 13, 541–549. doi: 10.1002/(SICI)1097-0061(199705)13:6<541::AID-YEA112>3.0.CO;2-4

Porzoor, A., and Macreadie, I. G. (2013). Application of yeast to study the tau and amyloid-beta abnormalities of Alzheimer's disease. *J. Alzheimers Dis.* 35, 217–225. doi: 10.3233/JAD-122035

Raab, M., Gentili, M., de Belly, H., Thiam, H. R., Vargas, P., Jimenez, A. J., et al. (2016). ESCRT III repairs nuclear envelope ruptures during cell migration to limit DNA damage and cell death. *Science (New York, N.Y.)* 352, 359–362. doi: 10.1126/science.aad7611

Rauk, A. (2008). Why is the amyloid beta peptide of Alzheimer's disease neurotoxic? *Dalton Trans.* 1273–1282. doi: 10.1039/b718601k

Ruan, L., Zhou, C., Jin, E., Kucharavy, A., Zhang, Y., Wen, Z., et al. (2017). Cytosolic proteostasis through importing of misfolded proteins into mitochondria. *Nature* 543, 443–446. doi: 10.1038/nature21695

Schindelin, J., Arganda-Carreras, I., Frise, E., Kaynig, V., Longair, M., Pietzsch, T., et al. (2012). Fiji: an open-source platform for biological-image analysis. *Nat. Methods* 9, 676–682. doi: 10.1038/nmeth.2019

Schreij, A. M., Fon, E. A., and McPherson, P. S. (2016). Endocytic membrane trafficking and neurodegenerative disease. *Cell Mol. Life Sci.* 73, 1529–1545. doi: 10.1007/s00018-015-2105-x

Shoshan-Barmatz, V., Nahon-Crystal, E., Shteinfer-Kuzmine, A., and Gupta, R. (2018). VDAC1, mitochondrial dysfunction, and Alzheimer's disease. *Pharmacol. Res.* 131, 87–101. doi: 10.1016/j.phrs.2018.03.010

Sun, Y., Rong, X., Lu, W., Peng, Y., Li, J., Xu, S., et al. (2015). Translational study of Alzheimer's disease (AD) biomarkers from brain tissues in AbetaPP/PS1 mice and serum of AD patients. *J. Alzheimers Dis.* 45, 269–282. doi: 10.3233/JAD-142805

Sundquist, W. I., and Ullman, K. S. (2015). Cell biology. an escrt to seal the envelope. *Science (New York, N.Y.)* 348, 1314–1315. doi: 10.1126/science.aac7083

Swinnen, E., Buttner, S., Outeiro, T. F., Galas, M. C., Madeo, F., Winderickx, J., et al. (2011). Aggresome formation and segregation of inclusions influence toxicity of alpha-synuclein and synphilin-1 in yeast. *Biochem. Soc. Trans.* 39, 1476–1481. doi: 10.1042/BST0391476

Swinnen, E., Wilms, T., Idkowiak-Baldys, J., Smets, B., De Snijder, P., Accardo, S., et al. (2014). The protein kinase Sch9 is a key regulator of sphingolipid metabolism in *Saccharomyces cerevisiae*. *Mol. Biol. Cell* 25, 196–211. doi: 10.1091/mbc.E13-06-0340

Tenreiro, S., Franssens, V., Winderickx, J., and Outeiro, T. F. (2017). Yeast models of Parkinson's disease-associated molecular pathologies. *Curr. Opin. Genet. Dev.* 44, 74–83. doi: 10.1016/j.gde.2017.01.013

Tenreiro, S., Munder, M. C., Alberti, S., and Outeiro, T. F. (2013). Harnessing the power of yeast to unravel the molecular basis of neurodegeneration. *J. Neurochem.* 127, 438–452. doi: 10.1111/jnc.12271

Thomas, R. S., Lelos, M. J., Good, M. A., and Kidd, E. J. (2011). Clathrin-mediated endocytic proteins are upregulated in the cortex of the Tg2576 mouse model of Alzheimer's disease-like amyloid pathology. *Biochem. Biophys. Res. Commun.* 415, 656–661. doi: 10.1016/j.bbrc.2011.10.131

Tong, A. H., Evangelista, M., Parsons, A. B., Xu, H., Bader, G. D., Page, N., et al. (2001). Systematic genetic analysis with ordered arrays of yeast deletion mutants. *Science* 294, 2364–2368. doi: 10.1126/science.1065810

Treusch, S., Hamamichi, S., Goodman, J. L., Matlack, K. E. S., Chung, C. Y., Baru, V., et al. (2011). Functional links between a toxicity, endocytic trafficking, and Alzheimer's disease risk factors in yeast. *Science* 334, 1241–1245. doi: 10.1126/science.1213210

Varadarajan, S., Bampton, E. T., Smalley, J. L., Tanaka, K., Caves, R. E., Butterworth, M., et al. (2012). A novel cellular stress response characterised by a rapid reorganisation of membranes of the endoplasmic reticulum. *Cell Death Differ.* 19, 1896–1907. doi: 10.1038/cdd.2012.108

Varadarajan, S., Tanaka, K., Smalley, J. L., Bampton, E. T., Pellecchia, M., Dinsdale, D., et al. (2013). Endoplasmic reticulum membrane reorganization is regulated by ionic homeostasis. *PLoS One* 8:e56603. doi: 10.1371/journal.pone.0056603

Verduyckt, M., Vignaud, H., Bynens, T., Van den Brande, J., Franssens, V., Cullin, C., et al. (2016). Yeast as a model for Alzheimer's disease: latest studies and advanced strategies. *Methods Mol. Biol.* 1303, 197–215. doi: 10.1007/978-1-4939-2627-5_11

Vevea, J. D., Garcia, E. J., Chan, R. B., Zhou, B., Schultz, M., Di Paolo, G., et al. (2015). Role for lipid droplet biogenesis and microlipophagy in adaptation to lipid imbalance in yeast. *Dev. Cell* 35, 584–599. doi: 10.1016/j.devcel.2015.11.010

Vicente Miranda, H., Gomes, M. A., Branco-Santos, J., Breda, C., Lázaro, D. F., Lopes, L. V., et al. (2016). Glycation potentiates neurodegeneration in models of Huntington's disease. *Sci. Rep.* 6:36798. doi: 10.1038/srep36798

Vignaud, H., Bobo, C., Lascu, I., Sörgjerd, K. M., Zako, T., Maeda, M., et al. (2013). A structure-toxicity study of Aß42 reveals a new anti-parallel aggregation pathway. *PLoS One* 8:e80262. doi: 10.1371/journal.pone.0080262

Viola, K. L., and Klein, W. L. (2015). Amyloid β oligomers in Alzheimer's disease pathogenesis, treatment, and diagnosis. *Acta Neuropathol.* 129, 183–206. doi: 10.1007/s00401-015-1386-3

Wang, D., Yuen, E. Y., Zhou, Y., Yan, Z., and Xiang, Y. K. (2011). Amyloid beta peptide-(1-42) induces internalization and degradation of beta2 adrenergic receptors in prefrontal cortical neurons. *J. Biol. Chem.* 286, 31852–31863. doi: 10.1074/jbc.M111.244335

Wang, H., Ma, J., Tan, Y., Wang, Z., Sheng, C., Chen, S., et al. (2010). Amyloid-β1-42 induces reactive oxygen species-mediated autophagic cell death in U87 and SH-SY5Y Cells. *J. Alzheimer's Dis.* 21, 597–610. doi: 10.3233/JAD-2010-091207

Willen, K., Edgar, J. R., Hasegawa, T., Tanaka, N., Futter, C. E., and Gouras, G. K. (2017). Abeta accumulation causes MVB enlargement and is modelled by dominant negative VPS4A. *Mol. Neurodegener.* 12:61. doi: 10.1186/s13024-017-0203-y

Winderickx, J., Delay, C., De Vos, A., Klinger, H., Pellens, K., Vanhelmont, T., et al. (2008). Protein folding diseases and neurodegeneration: lessons learned from yeast. *Biochim. Biophys. Acta* 1783, 1381–1395. doi: 10.1016/j.bbamcr.2008.01.020

Xiang, Y., Lam, S. M., and Shui, G. (2015). What can lipidomics tell us about the pathogenesis of Alzheimer disease? *Biol. Chem.* 396, 1281–1291. doi: 10.1515/hsz-2015-0207

Xu, W., Fang, F., Ding, J., and Wu, C. (2018). Dysregulation of Rab5-mediated endocytic pathways in Alzheimer's disease. *Traffic* 19, 253–262. doi: 10.1111/tra.12547

Yamazaki, Y., Takahashi, T., Hiji, M., Kurashige, T., Izumi, Y., Yamawaki, T., et al. (2010). Immunopositivity for ESCRT-III subunit CHMP2B in granulovacuolar degeneration of neurons in the Alzheimer's disease hippocampus. *Neurosci. Lett.* 477, 86–90. doi: 10.1016/j.neulet.2010.04.038

Yang, D. S., Stavrides, P., Saito, M., Kumar, A., Rodriguez-Navarro, J. A., Pawlik, M., et al. (2014). Defective macroautophagic turnover of brain lipids in the TgCRND8 Alzheimer mouse model: prevention by correcting lysosomal proteolytic deficits. *Brain* 137(Pt 12), 3300–3318. doi: 10.1093/brain/awu278

Zabrocki, P., Pellens, K., Vanhelmont, T., Vandebroek, T., Griffioen, G., Wera, S., et al. (2005). Characterization of alpha-synuclein aggregation and synergistic toxicity with protein tau in yeast. *FEBS J.* 272, 1386–1400. doi: 10.1111/j.1742-4658.2005.04571.x

Conflict of Interest Statement: The authors declare that the research was conducted in the absence of any commercial or financial relationships that could be construed as a potential conflict of interest.